Article

Cell

Molecular Basis of Arthritogenic Alphavirus Receptor MXRA8 Binding to Chikungunya Virus Envelope Protein

Graphical Abstract

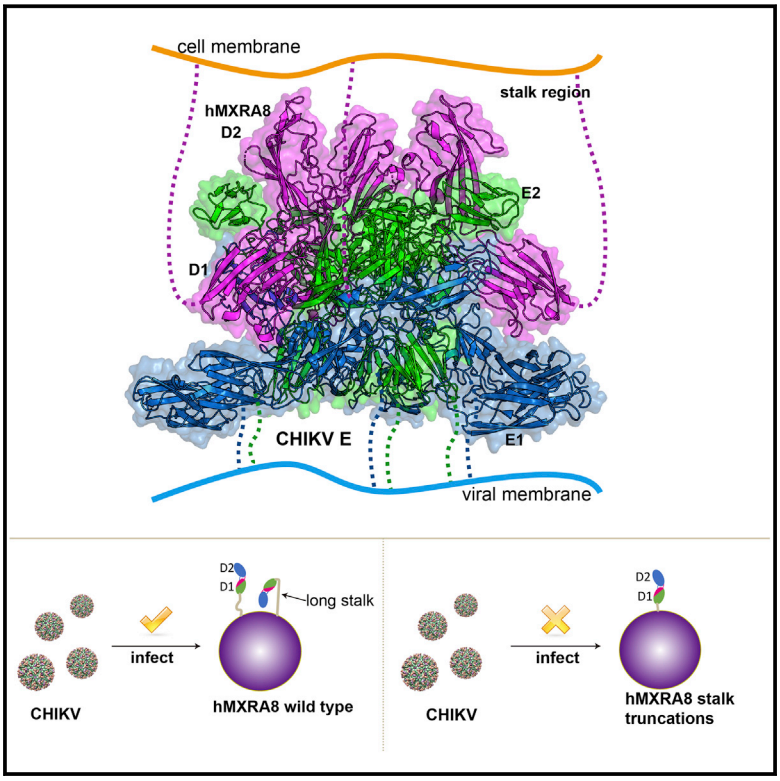

Highlights

- MXRA8 has two Ig-like domains with an unexpected structural topology
- MXRA8 binds in the "canyon" between two protomers of the CHIKV E spike
- Both the two domains and hinge region of MXRA8 are involved in interaction
- The stalk region of MXRA8 is critical for CHIKV virus entry

Authors

Hao Song, Zhennan Zhao, Yan Chai, ..., Jianxun Qi, Feng Gao, George F. Gao

Correspondence

gaofeng@tib.cas.cn (F.G.), gaof@im.ac.cn (G.F.G.)

In Brief

Structural insights into how Chikungunya virus binds its receptor on human cells provides a guide for developing antiviral therapies against arthritogenic alphaviruses.

Song et al., 2019, Cell *177*, 1714–1724
June 13, 2019
https://doi.org/10.1016/j.cell.2019.04.008

CellPress

Cell

Article

Molecular Basis of Arthritogenic Alphavirus Receptor MXRA8 Binding to Chikungunya Virus Envelope Protein

Hao Song,[1,13] Zhennan Zhao,[2,3,13] Yan Chai,[2,13] Xiyue Jin,[2,4] Changyao Li,[5] Fei Yuan,[2] Sheng Liu,[2,4] Zhengrong Gao,[6] Haiyuan Wang,[7] Jian Song,[2] Leonardo Vazquez,[2,8] Yanfang Zhang,[2,3] Shuguang Tan,[2] Carlos M. Morel,[8] Jinghua Yan,[2] Yi Shi,[2,3,9] Jianxun Qi,[2,3] Feng Gao,[10,11,*] and George F. Gao[1,2,3,4,9,10,12,14,*]

[1]Research Network of Immunity and Health (RNIH), Beijing Institutes of Life Science, Chinese Academy of Sciences, Beijing 100101, China
[2]CAS Key Laboratory of Pathogenic Microbiology and Immunology, Institute of Microbiology, Chinese Academy of Sciences, Beijing 100101, China
[3]Savaid Medical School, University of Chinese Academy of Sciences, Beijing 100049, China
[4]School of Life Sciences, University of Science and Technology of China, Hefei, Anhui 230026, China
[5]College of Veterinary Medicine, China Agricultural University, Beijing 100193, China
[6]Kunming Institute of Zoology, Chinese Academy of Sciences, Kunming 650223, China
[7]College of Animal Sciences and Technology, Guangxi University, Nanning 530004, China
[8]National Institute of Science and Technology for Innovation on Diseases of Neglected Populations (INCT-IDPN), Center for Technological Development in Health (CDTS), Oswaldo Cruz Foundation (Fiocruz), Rio de Janeiro, Rio de Janeiro 21040-361, Brazil
[9]CAS Center for Influenza Research and Early-warning (CASCIRE), Chinese Academy of Sciences, Beijing 100101, China
[10]Tianjin Institute of Industrial Biotechnology, Chinese Academy of Sciences, Tianjin 300308, China
[11]Institute of Genetics and Developmental Biology, Chinese Academy of Sciences, Beijing 100101, China
[12]National Institute for Viral Disease Control and Prevention, Chinese Center for Disease Control and Prevention (China CDC), Beijing 102206, China
[13]These authors contributed equally
[14]Lead Contact
*Correspondence: gaofeng@tib.cas.cn (F.G.), gaof@im.ac.cn (G.F.G.)
https://doi.org/10.1016/j.cell.2019.04.008

SUMMARY

Arthritogenic alphaviruses, such as Chikungunya virus (CHIKV), cause severe and debilitating rheumatic diseases worldwide, resulting in severe morbidity and economic costs. Recently, MXRA8 was reported as an entry receptor. Here, we present the crystal structures of the mouse MXRA8, human MXRA8 in complex with the CHIKV E protein, and the cryo-electron microscopy structure of human MXRA8 and CHIKV virus-like particle. MXRA8 has two Ig-like domains with unique structural topologies. This receptor binds in the "canyon" between two protomers of the E spike on the surface of the virion. The atomic details at the interface between the two binding entities reveal that both the two domains and the hinge region of MXRA8 are involved in interaction with CHIKV E1-E2 residues from two protomers. Notably, the stalk region of MXRA8 is critical for CHIKV virus entry. This finding provides important information regarding the development of therapeutic countermeasures against those arthritogenic alphaviruses.

INTRODUCTION

Alphaviruses are a group of enveloped RNA viruses, which are mainly transmitted by mosquitoes and which cause outbreaks of many human and animal diseases; alphaviral manifestations vary from fever or rash to significant inflammatory pathologies, including encephalitis and severe arthritis (Chen et al., 2015; Gao, 2018; Suhrbier et al., 2012). Encephalitic alphaviruses, such as Eastern equine encephalitis virus (EEEV), Venezuelan equine encephalitis virus (VEEV), and Western equine encephalitis virus (WEEV), are neuroinvasive and frequently cause encephalitis (Ronca et al., 2016). In contrast, arthritogenic alphaviruses, such as Chikungunya virus (CHIKV), Ross River virus (RRV), Mayaro virus (MAYV), and O'nyong-nyong virus (ONNV), cause severe arthralgia (Mejía and López-Vélez, 2018). These viruses cause endemic diseases and occasionally trigger large epidemics (Suhrbier et al., 2012). One of these, CHIKV, is a serious disease in many tropical and subtropical countries throughout the world; there was a recent CHIKV outbreak in Brazil (Gérardin et al., 2018). The CHIKV infection is characterized by acute and chronic symmetrical peripheral polyarthralgia-polyarthritis, and severe diseases, even fatalities, have been reported in recent outbreaks (Zanotto and Leite, 2018). However, no licensed vaccine or antiviral therapy is available (Zanotto and Leite, 2018).

Alphaviral invasions of susceptible cells are mediated by the envelope (E) glycoproteins, which form icosahedral shells at the virion surfaces (Sun et al., 2013). Like other alphaviruses, CHIKV entry is mediated by two glycoproteins, E1 and E2, on the surface of the virion; these glycoproteins, particularly E2, are the main targets of the antibody response (Fox et al., 2015). It is believed that the glycoprotein E2, derived from the cellular furin cleavage of the p62 precursor into E3 and E2, is responsible for receptor binding, while E1 is responsible for

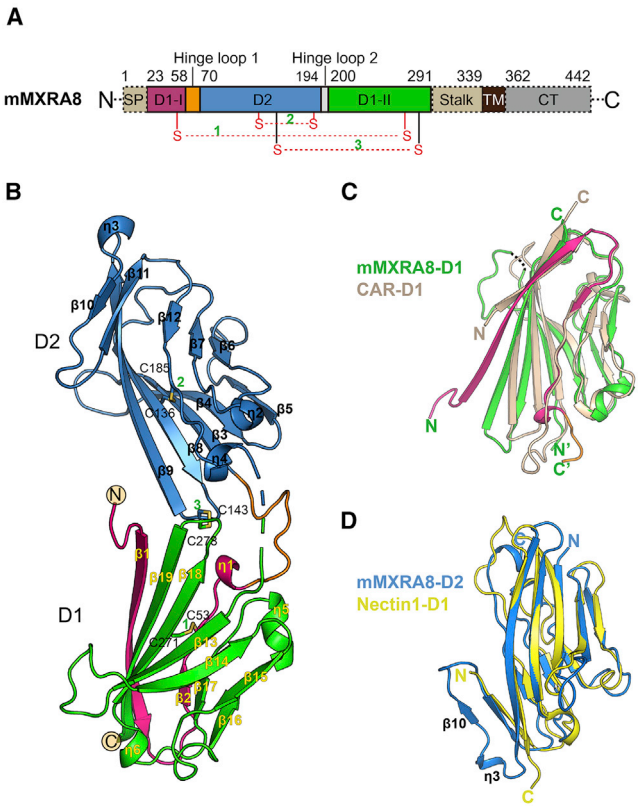

Figure 1. Overall Structure of the Ectodomain of Mouse MXRA8

(A) A schematic representation of the mouse MXRA8 (mMXRA8) protein. Signal peptide (SP), transmembrane region (TM), and C-terminal cytoplasmic tail domain (CT). The three disulfide bonds are highlighted in red.

(B) A cartoon representation of the ectodomain of mMXRA8. The secondary structural elements are labeled, and the disulfide bonds are shown as orange sticks.

(C) Superimposition of the D1 Ig domain of the mMXRA8 ectodomain with the V-set CAR D1 Ig domain (PDB: 3J6N).

(D) Superimposition of the D2 Ig domain of the mMXRA8 ectodomain with the V-set Nectin1 D1 Ig domain (PDB: 4FMF).

See also Figures S1 and S3 and Table S1.

membrane fusion (Voss et al., 2010). The newly synthesized p62 glycoproteins interact with E1 to form heterodimers, which subsequently trimerize into a viral spike in the endoplasmic reticulum (ER). The viral spike is then cleaved by furin to release E3 during transportation from the acidic environment of the Golgi and the early endosomes to the neutral pH environment of the cell surface (Lescar et al., 2001). E3 may facilitate the formation of the p62-E1 heterodimers and then prevent the premature exposure of the E1 fusion loops due to fusogenic activation (Li et al., 2010; Voss et al., 2010; Yap et al., 2017). Previous studies have described the crystal structures of the p62-E1 heterodimer, the mature E3-E2-E1 heterotrimer glycoprotein, and the Sindbis virus (SINV) E2-E1 heterodimer in acidic environments (Li et al., 2010; Voss et al., 2010). These studies have provided important insights into the organization of the E protein, into the acid-triggered conformational change of the virus particle, and into the built-in inhibition mechanism in the immature viral complex.

A recent study showed that multiple emerging arthritogenic alphaviruses, including CHIKV, RRV, MAYV, and ONNV, use MXRA8 as a functional receptor (Zhang et al., 2018). How this receptor binds the envelope protein is the key question to be addressed in this study, which will be helpful for the development of countermeasures against these viruses and the understanding of the viral entry into the cells.

MXRA8, also called DICAM, ASP3, or limitrin, is an adhesion molecule expressed on epithelial, myeloid, and mesenchymal cells (Jung et al., 2008, 2012; Yonezawa et al., 2003). Sequence alignment predicts that MXRA8 has two V-type Ig domains in its ectodomain and may share homology with other adhesion molecules, including the junctional adhesion molecule (JAM), which is a reovirus entry receptor (Barton et al., 2001), and the nectin1 molecule, a herpes simplex virus entry receptor (Geraghty et al., 1998; Lu et al., 2014).

Here, we report the crystal structures of the free mouse MXRA8 (mMXRA8) and the complex between human MXRA8 (hMXRA8) and the CHIKV E protein. We found that MXRA8 has two Ig-like domains that display unique structural topologies, different from those of the previously described two-domain Ig-like molecules. Domain 1 (D1) is formed by two discrete fragments, while the region between these two fragments consists of the hinge region and domain 2 (D2); that is, the linear protein sequence crosses the two domains. Therefore, the two Ig-like domains are connected by two hinge loops, as well as by an inter-domain disulfide bond. The binding mode of MXRA8 to CHIKV E is also unique. MXRA8 binds in the "canyon" between two protomers of the E spike on the virion surface, with the involvement of both the E1 and the E2 proteins. The atomic details of the interface between the two binding entities reveal that the two domains and the MXRA8 hinge region all interact with the CHIKV E1-E2 residues from two protomers. The critical interactions observed in the complex structure were further demonstrated by site-directed alanine-scanning mutagenesis and surface plasmon resonance (SPR) experiments. In addition, we showed that the stalk region of MXRA8 was necessary for efficient binding and entry. The identification of multiple binding interfaces for receptor-envelope interaction might inform the development of novel vaccines and broadly neutralizing antibodies. Our findings will help to drive the development of powerful antiviral reagents against arthritogenic alphaviruses.

RESULTS AND DISCUSSION

Structure of mMXRA8

Here, we constructed the ectodomains of both human and mouse MXRA8 proteins into *p*ET21a expression vectors. We then produced soluble proteins by the refolding method (Figures S1A and S1B) (Li et al., 2005). Both MXRA8 proteins exist as monomers in solution (Figures S1C and S1D). The human and mouse MXRA8 proteins share a sequence identity of about 80%. Subsequently, we crystallized and obtained diffracting crystals for mMXRA8, and then determined its 2.4-Å-resolution structure (Table S1). The structure shows that the mMXRA8 has two Ig-like domains. However, these two domains are arranged in a unique structural topology, different from all the other

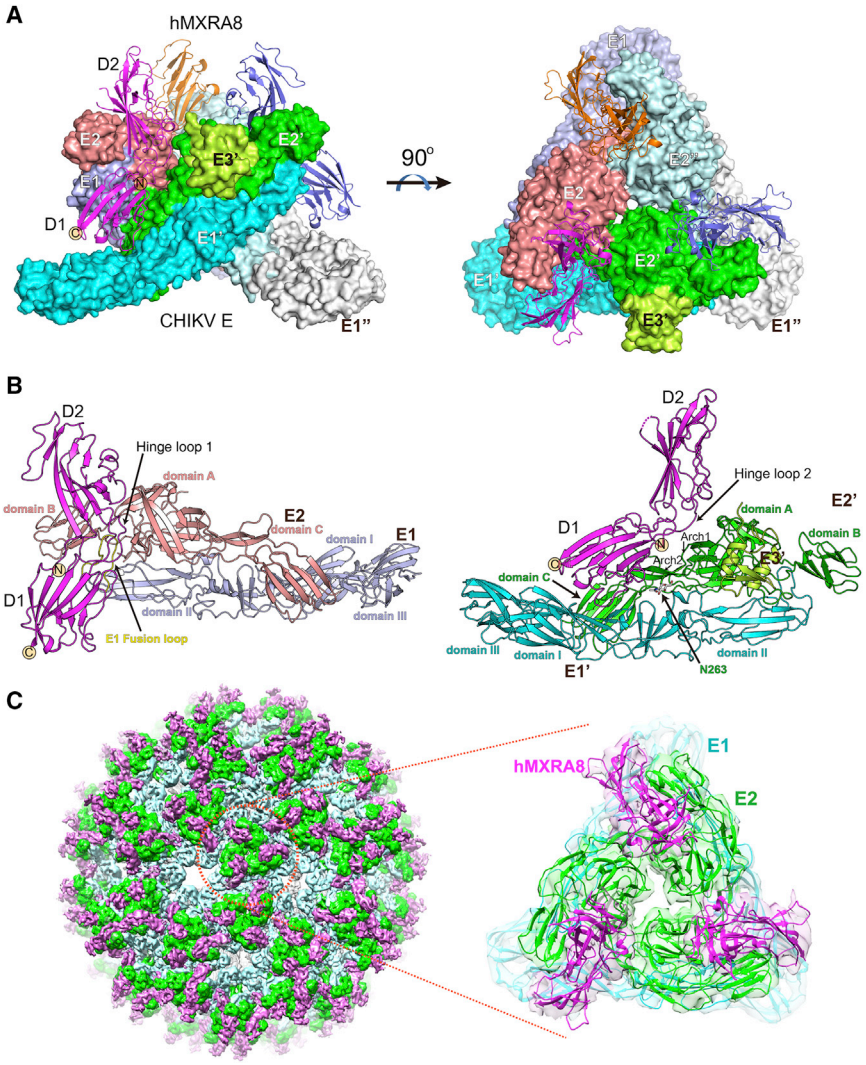

Figure 2. The Complex Structure of CHIKV E3-E2-E1 Glycoprotein Bound to Human MXRA8

(A) An overall representation of the complex crystal structure. Three CHIKV E3-E2-E1 molecules forming the trimer spike are shown in surface representation. The E1 domains of three molecules are shown in light blue, cyan, and white. The E2 domains are shown in salmon, green, and pale blue. Only one E3 domain was observed in the structure, which is shown here in lemon. The three human MXRA8 (hMXRA8) molecules are shown in a ribbon and are colored magenta, yellow-orange, and sky blue (color names as given by PyMOL). The 90° rotation on the right panel shows the top view of the complex.

(B) Ribbon diagrams of one hMXRA8 molecule binds to two E proteins in distinct binding modes. The fusion loop of the E1 protein is highlighted in yellow.

(C) Overall view of the cryo-EM complex structure of hMXRA8 bound to the CHIKV VLP particle at a resolution of 8.9 Å. E1 is shown in cyan, E2 is shown in green, and hMXRA8 is shown in magenta. The virion map is represented as a gray transparent surface at the right panel. The hMXRA8 and CHIKV E1-E2 complex fit well in the map, while hMXRA8 binds to the "canyon" region between two adjacent protomers in one spike. The E3 protein was not apparent in the cryo-EM density map.

See also Figures S2, S3, and S4 and Table S1.

structure-known 2-Ig-like molecules. The D1 is formed by two discrete fragments, while the region between these two fragments is made up of the hinge region and D2 (i.e., the linear protein sequences cross the two domains) (Figure 1A). The first fragment of D1 (D1-I) contains three secondary elements, two β strands (β1 and β2) and one 3_{10} helix (η1), covering residues from 23–58 (Figures 1A and 1B). The hinge region consists of two loops, one formed by residues 59–69 and the other by residues 195–199, which is disordered in structure (Figures 1A and 1B). The D2 is formed by residues 70–194, including ten β strands (β3–β12) and three 3_{10} helices (η2, η3, and η4) (Figures 1A and 1B). The second fragment of D1 (D1-II) covers residues 200–291, containing seven β strands (β13–β19) and two 3_{10} helices (η5 and η6) (Figures 1A and 1B). In addition to the ectodomain, the mMXRA8 also has a 48-residue stalk region, a 23-residue transmembrane region, and an 81-residue cytoplasmic tail (Figure 1A). A total of three disulfide bonds in the mMXRA8 structure are defined. The first one is in D1, formed by residues C53 and C271, and the second one is in D2, formed by residues C136 and C185 (Figures 1A and 1B). The third one is formed by C143 (in D2) and C278 (in D1) near the hinge region, which may limit the flexibility of the hinge between the D1 and D2. This structure is unique among other structure-known 2-Ig-like molecules (Figures 1A and 1B). Consistent with this observation, separate refolding of the two Ig-like domains based on linear sequences according to the earlier prediction studies (Jung et al., 2008, 2012; Yonezawa et al., 2003) (hMXRA8-pD1, G25-G158; hMXRA8-pD2, P159-A292) did not yield any soluble Ig-like proteins (Figures S1E and S1F).

Structural alignments on the Dali server (Holm and Rosenström, 2010) reveals that the structural fold of mMXRA8-D1 most closely resembles that of D1 from the Coxsackie and adenovirus receptor (CAR) (Figure 1C), which is the primary cellular receptor for group B coxsackie viruses and most of the adenoviruses (Bewley et al., 1999). CAR D1 plays a crucial role in adenoviral gene therapy (Kirby et al., 2000). By contrast, the structural fold of mMXRA8-D2 most closely resembles that of D1 from nectin1 (Lu et al., 2014; Zhang et al., 2011) (Figure 1D), even though it has an extra region (η3 and β10). MXRA8 can thus be considered an unconventional Ig-like molecule receptor, with an unexpected structural topology and a unique inter-domain assembly. However, the overall folds of the MXRA8 domains are similar to those of other adhesion molecules.

Table 1. Interaction between hMXRA8 and CHIKV E3-E2-E1

hMXRA8		Contacts[a]	CHIKV	Total Contacts
			E2	
D1-D2 hinge region (loop1)	P57	5	D223	81
	Q63	3, 14, 1, 8	H18 (1)[b], S27 (1), C28, H29	
	D64	16, 6, 2	H26, S27 (1), C28	
	L66	1	C28	
	D68	3, 2	I121, H123	
	R69	15, 5	N72 (2), H123	
D2	D76	1	T191	165
	P84	3	D214	
	A85	2, 1, 2, 11	T191, V192, N193, D214 (1)	
	R86	2	N193	
	R87	5, 13	T179 (1), N193	
	D90	4	R119	
	Y92	4, 8, 14	D71 (1), N72 (1), R119	
	A94	2	I121	
	G95	5	R119	
	E96	14, 9	R119 (1), K120	
	Q97	1	R119	
	R98	5, 6, 3, 5, 8	D71, M74 (1), P75 (1), A76, R119	
	Y100	1, 2	M74, N193	
	H140	10, 1	T179, M181	
	H142	1, 3	R178, T179	
	H145	7	R178 (1)	
	Y147	1, 11	M181, S182 (1)	
			E1	
D1-D2 hinge region (loop1)	Q55	3	D97 (1)	25
	V60	2	F87	
	T62	3, 8	G227, Y87	
	Q63	1	G227	
	R65	6, 2	W89 (2), G91	
D1	D248	4	A226	35
	E251	5, 2, 3, 3	A226 (1), G227, Y85, F87	
	R252	4, 5, 7, 2	G83 (1), V84 (1), Y85, D97 (1)	
			E2′	
D2	D116	9	W64 (1)	9
D1-D2 hinge region (loop2)	R196	6	W64	17
	H197	1, 6	S159, T160	
	V198	1	S159	
	E199	2	Q158	
	Q202	1	V157	
D1	S228	7, 10	V264, T265 (1)	34
	G229	5	T265 (1)	
	E230	10, 2	N263 (2), NAG	

(*Continued on next page*)

Table 1. *Continued*

hMXRA8		Contacts[a]	CHIKV	Total Contacts
			E1′	
D1	L237	4	E39	25
	F238	1, 2, 5	S130, T145, T147	
	R240	4, 4	N264 (1), P265	
	D241	5	K132 (1)	

[a]Numbers represent the number of atom-to-atom contacts between the hMXRA8 residues and CHIKV E3-E2-E1 residues, which were analyzed by the contact program in CCP4 suite (the distance cutoff is 4.5 Å).
[b]Numbers in the parentheses represent the number of potential hydrogen bonds between the hMXRA8 residues and CHIKV E3-E2-E1 residues.

Overall Structure of the hMXRA8 and CHIKV E Complex

We expressed and obtained the CHIKV E3-E2-E1 protein complex as previously reported (Figure S1G) (Voss et al., 2010). The crystal screen with the complexes between hMXRA8 and the E3-E2-E1 protein yielded some diffracting crystals. The structure was determined by molecular replacement (MR), using the above-described mMXRA8 structure and the previously reported CHIKV E structure (Voss et al., 2010) as models. The final complex structure was determined to a resolution of 3.49 Å (Table S1), and the E3-E2-E1 homotrimer complexed with three hMXRA8 molecules was observed in one asymmetric unit of the structure (Figure 2A). Only one protomer (representing one E3-E2-E1 or E2-E1) in the homotrimer has clear electronic density for E3, and the other two E3s are disordered in the structure. The hMXRA8 and E3-E2-E1 proteins interact with each other in a 3:3 binding mode (Figure 2A). Three hMXRA8 proteins bind to the trimeric spike, and each hMXRA8 interacts with two adjacent protomers with distinct binding sites (Figures 2A and 2B). For one protomer, the D2 and the hinge region of hMXRA8 bind to domain A and domain B of E2, whereas the D1 and the first hinge loop of hMXRA8 bind to the fusion loop (FL) and domain II of the E1 molecule. For the other protomer, the D1, D2, and second hinge loop of hMXRA8 bind to arch1, arch2, and domain A of the E2 molecule, and the D1 of hMXRA8 binds to domain I and domain II of the E1 molecule (Figure 2B). E3 is not involved in hMXRA8 binding. We also determined the

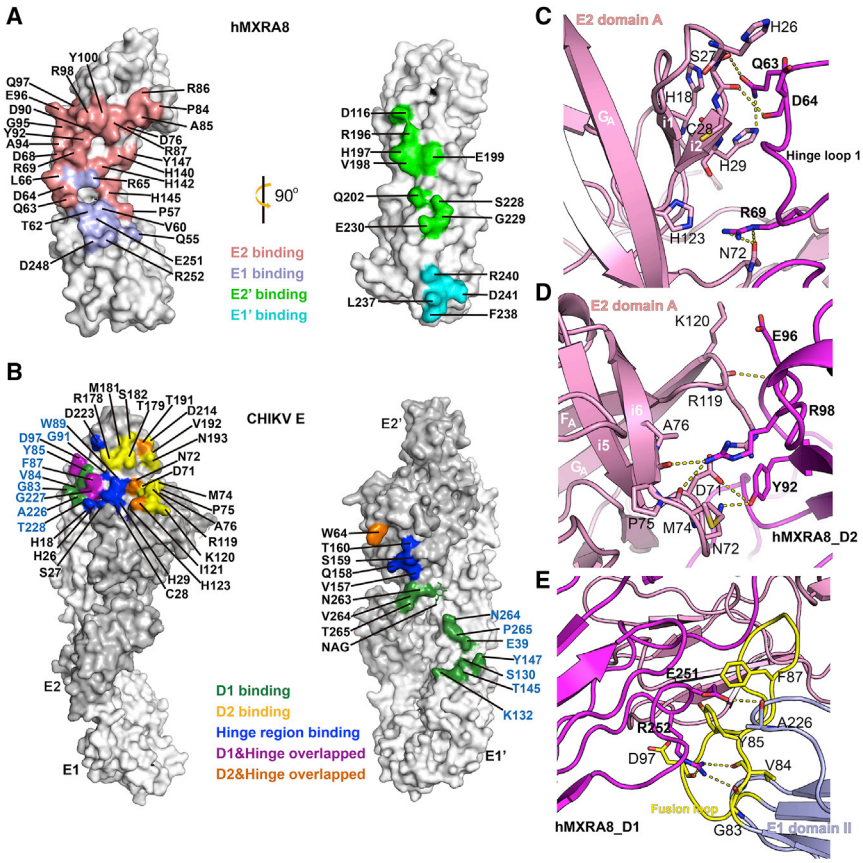

Figure 3. Contact Residues at the Binding Interface

(A) Contact residues of the binding interface in the hMXRA8 protein.
(B) Contact residues of the binding interface in the CHIKV E proteins.
(C) Detailed interactions between hMXRA8 hinge loop 1 and CHIKV E2 domain A.
(D) Detailed interactions between hMXRA8 D2 and CHIKV E2 domain A.
(E) Detailed interactions between hMXRA8 D1 and CHIKV E1 fusion loop.
See also Figures S5 and S6.

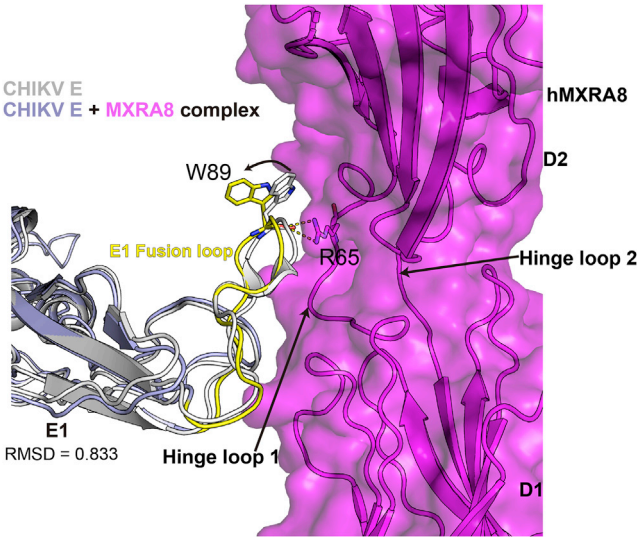

Figure 4. Structural Comparison of CHIKV E1 FL with and without Its Receptor hMXRA8 Aligned Based on the E1 Domain

The FL of CHIKV E1 (light blue) bound to hMXRA8 (magenta) is highlighted in yellow, and the CHIKV E1 apo (PDB: 3N41) (Voss et al., 2010) is colored gray. Residue W89 in E1 FL region forms two potential hydrogen bond interactions with R65 in the hinge loop of hMXRA8. The side chain of residue W89 in the FL region rotates against MXRA8 after binding.

cryo-electron microscopy (cryo-EM) structure of the hMXRA8 complex with CHIKV virus-like particles (VLPs) at a resolution of 8.9 Å (Figures S2A and S2B). The hMXRA8 and CHIKV E1-E2 complex fit well in the map, and hMXRA8 binds to the "canyon" region between two adjacent protomers in one spike (Figures 2C and S2C). The E3 protein was not apparent in the cryo-EM density map, which is consistent with the previously reported CHIKV VLP cryo-EM structures (Sun et al., 2013). We also analyzed the crystal packing of MXRA8 molecules in our crystal structure and found that the weak interaction from crystal packing will not influence the orientation of binding MXRA8 (Figures S2D–S2H). This result is consistent with our cryo-EM structure that has the same binding orientation.

Multiple Interfaces between hMXRA8 and CHIKV E

We then further analyzed the binding details at the interfaces between the CHIKV E protein and hMXRA8. We found that 43 amino acids from hMXRA8 were involved in the interaction (Table 1). Over half of these residues are hydrophilic amino acids (polar or charged), indicating the binding of CHIKV E to hMXRA8 is dominated by polar contacts. hMXRA8 binds to two E3-E2-E1 protomers with a buried area of 2,181 Å^2. The major interaction is made by the E2 molecule in one protomer with a buried area of 1,176 Å^2 and 62.9% of atom-to-atom contacts, while the E1 molecule in one promoter, as well as the E2′ and E1′ molecules in the other protomer (representing E′), contribute less binding (380 Å^2, 388 Å^2, and 237 Å^2, respectively) (Table 1). Residues (Q63, D64, and R69) in the hinge region and residues (A85, R87, Y92, E96, R98, and Y100) in the D2 region of hMXRA8 are predominantly involved in E2 binding (Figure 3A; Table 1). Residues (T62 and R65) in the hinge region and residues (D248, E251, and R252) in the D1 region of hMXRA8 are involved in E1 binding. By contrast, E2′ and E1′ molecules in the other protomer bind to another side of hMXRA8 with minor interactions, including the residues in the hinge region and D1. Notably, residues Q63, D64, and R69 in the hinge region of hMXRA8, as well as residues Y92, E96, and R98 in the D2 region, form multiple potential hydrogen bond interactions with residues in CHIKV E2 domain A (Figures 3C and 3D; Table 1). The hMXRA8 also interacts with the FL region (residues G83, V84, Y85, F87, W89, G91, and D97), and the domain II (residues A226, G227, and T228) of E1 (Figures 3E and S3B). Residues E251 and R252, in the D1 region of hMXRA8, participate in potential hydrogen bond interactions with amino acids in the E1 FL region (Figure 3E). Clearly, the receptor-binding sites on the E proteins identified here, in our complex structure, are more abundant than those (including domain A and domain B of the E2 protein) previously identified by neutralizing antibody mapping (Figure 3B) (Fox et al., 2015; Long et al., 2015; Smith et al., 2015; Sun et al., 2013). This indicates that there is plenty of scope for future research on neutralization antibody identification. Overall, the virus-receptor engagement is dominated by the polar contacts mediated by the hydrophilic residues with multiple binding sites, and the interface is enlarged by the 3:3 binding mode to enhance the viral attachment.

A previous mutagenesis mapping study demonstrated that amino acids in the A and B domains of E2 contribute to the interaction between CHIKV and MXRA8; it was suggested that MXRA8 might bind to the surface-exposed region of the E2 protein (Zhang et al., 2018). Our study expands this view of the binding mode and interface. We also showed that residues W64, D71, and I121 in the E2 A domain, initially identified with mapping experiments (Zhang et al., 2018), are located in the binding sites (Figure 3B).

Comparisons between unbound CHIKV-E (Voss et al., 2010) and hMXRA8-bound CHIKV-E indicated that the overall folds of E1 and E2 are similar, with no apparent substantial conformational changes. Indeed, the root-mean-square deviation (RMSD) of E1 was 0.833 Å (for 374 Cα atoms) and of E2 was 0.978 Å (for 363 Cα atoms). The E1 FL region shifted only slightly after binding. We observed a conformational change in the side chain of residue W89 in the FL region after binding to MXRA8 (Figure 4). We also compared the structures of mMXRA8 and hMXRA8 and found that the inter-domain angle of D1-D2 shifted 15° between mMXRA8 and hMXRA8 (Figure S4A), although each domain maintained similar folds. As no apo hMXRA8 structure is yet available, it is unclear whether the conformational change occurs when this molecule binds to CHIKV E. We speculate that MXRA8 has flexibility of the inter-domain angle because of the two hinge loops, but the flexibility is limited due to the inter-domain disulfide bond.

A previous study has revealed that MXRA8 can bind to CHIKV, ONNV, RRV, MAYV, and Barmah Forest virus (BFV), and can partially interact with Semliki Forest virus (SFV), but cannot bind to SINV and VEEV (Zhang et al., 2018). Here, we analyzed the binding sites in the CHIKV E proteins based on the sequence alignment with these eight alphaviruses. We

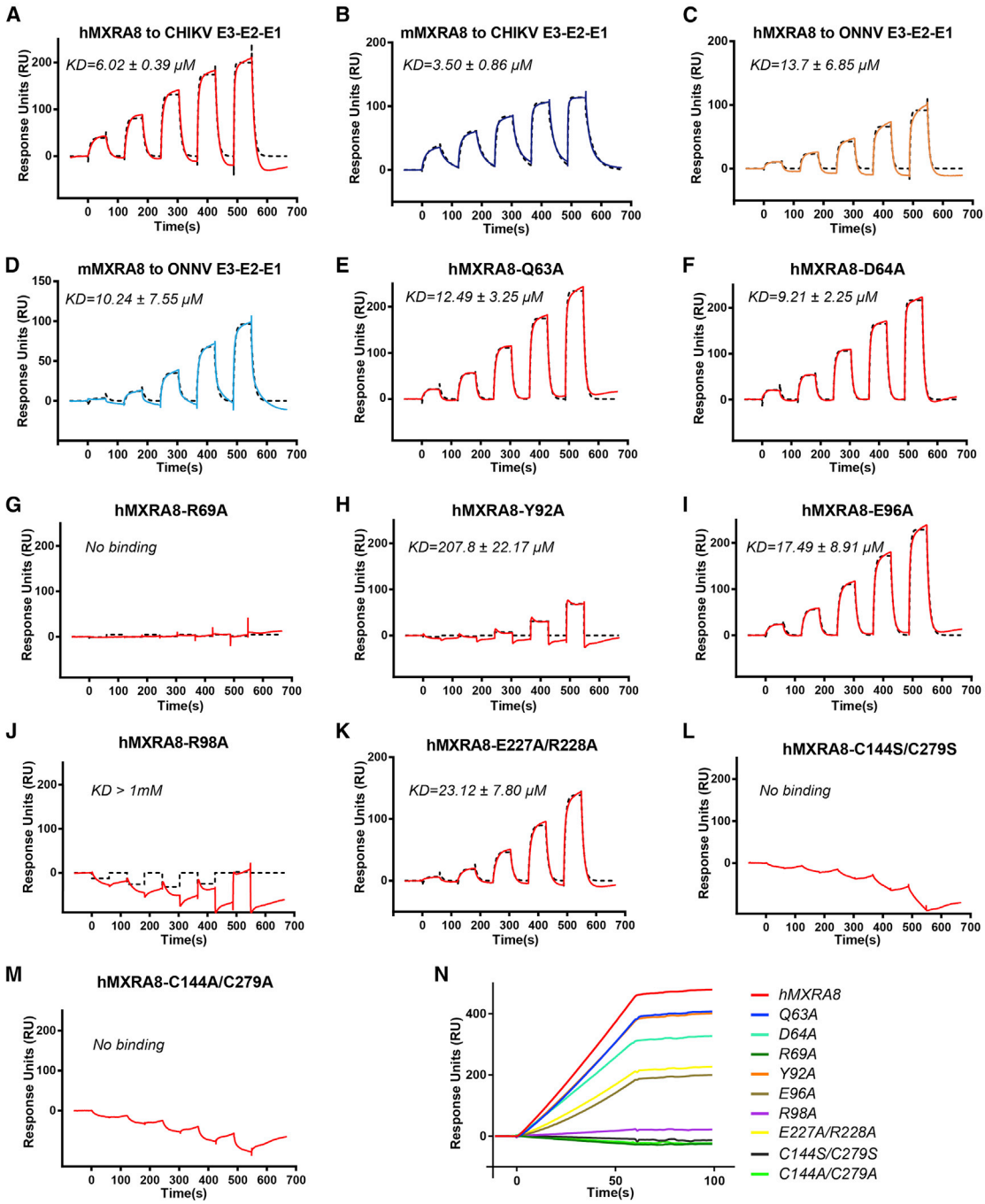

Figure 5. Binding Affinities between MXRA8 and Alphavirus E Proteins and Mutagenesis

(A–D) Specific interactions between human or mouse MXRA8 and E proteins from different alphaviruses, including CHIKV and ONNV characterized by SPR (A, hMXRA8 to CHIKV E; B, mMXRA8 to CHKV E; C, hMXRA8 to ONNV E; D, mMXRA8 to ONNV E). The indicated E proteins were captured on the chip immobilized with anti-His tag antibodies and tested for binding with gradient concentrations of MXRA8 (1.25 μM, 2.5 μM, 5 μM, 10 μM, and 20 μM) in single cycle mode. The binding profiles are shown with time (s) on the x axis and response units (RU) on the y axis. The black dotted curves were obtained by fitting data to the 1:1 binding model (BIAcore T100 Evaluation software). KD values shown are the mean ± SEM of three independent experiments.

(E–M) SPR assay showing the binding between different hMXRA8 mutant proteins (E) Q63A, (F) D64A, (G) R69A, (H) Y92A, (I) E96A, (J) R98A, (K) E227A/R228A, (L) C144S/C279S, (M) C144A/C279A, and the CHIKV E3-E2-E1 protein. The concentrations of mutant MXRA8s were the same as that of the

(legend continued on next page)

found that the residues at positions 18, 23, 76, 159, 160, and 178 in the E2 molecule are important for its differential binding capacities to MXRA8 (Figure S5). The side-chain characteristics of these residues are partially changed in SFV but are dramatically changed in SINV and VEEV (Figure S5). Zhang et al. (2018) also reported strain-to-strain variation on MXRA8-dependence for cellular entry, indicating that some strains like LR2006 can enter MXRA8 knockout cells because of heparan sulfate binding activity. We then analyzed the binding sites of representative CHIKV strains: 05-115, 119067, 181-25, LR2006, and AF15561 (Figure S6). Most of the receptor-binding residues are conserved, except residues at positions 145 and 226 in the E1 molecule, and residues at positions 72, 74, 157, 182, and 264 in the E2 molecule. Interestingly, the single mutation A226V may be associated with adaptation and enhanced transmission by the mosquito *Aedes albopictus* in the regions where *Aedes aegypti* is absent (Arias-Goeta et al., 2013). Future studies should investigate whether these variations in receptor-binding sites have biological functions or alter pathogenesis.

We tested the binding affinities of the CHIKV E protein to the hMXRA8 or mMXRA8 by the surface plasmon resonance (SPR) method and found that the binding affinities are similar between hMXRA8 and mMXRA8, ranging in micromolar levels (6.02 ± 0.39 μM versus 3.50 ± 0.86 μM) (Figures 5A and 5B). For the ONNV E protein, the values of the binding affinity to hMXRA8 and mMXRA8 are 13.7 ± 6.85 μM and 10.24 ± 7.55 μM (Figures 5C and 5D), respectively, which are slightly weaker than that of the CHIKV E protein. The binding affinities are lower than those (≈200 nM) observed in the binding between VLPs and mMXRA8 (Zhang et al., 2018), which might be due to increased binding avidity with the multiple E spikes on the surface of VLPs.

Mutagenesis of the Key Interaction Residues

In order to investigate the role of the above-described key residues involved in interactions between CHIKV E and its receptor, we performed site-directed mutagenesis and subsequent SPR experiments (Figures 5 and S7). We tested the contributions of residues Q63, D64, R69, Y92, E96, R98, E227, and R228 to the hMXRA8 binding of CHIKV E. These residues are key interacting residues of MXRA8, with high contact numbers and potential hydrogen bond interactions with CHIKV E (Figure 3; Table 1). Of note, single substitutions of Q63, D64, and E96 with alanine (A), and double substitution with E227A/R228A, slightly reduced the binding affinity for the CHIKV E interaction (Figures 5E, 5F, 5I and 5K); single-substitution of Y92A partially reduced the binding (Figure 5H). However, single substitutions of R69A and R98A completely abolished the binding (Figures 5G, 5H, and 5J). Notably, we found that the loss of the inter-domain disulfide bond in hMXRA8 (C144A/C279A or C144S/C279S) disrupted the binding to CHIKV E, indicating that this disulfide bond is essential to stabilizing the conformation of hMXRA8 D1, D2, and its hinge region to allow CHIKV E binding (Figures 5L and 5M). In addition, we also tested the binding of hMXRA8 mutants to CHIKV VLP using SPR, and showed that the single-substitutions of R69A and R98A, as well as inter-domain disulfide bond disruption, completely abolished virion binding (Figure 5N). This is consistent with the binding between hMXRA8 mutants and the CHIKV E protein.

The Stalk Region of MXRA8

As a type I transmembrane protein, MXRA8 differs from other proteins due to its unique domain organization. The N-terminal D1, which is thought to be the domain most distal from the cell surface proteins (e.g., JAM), is the most membrane-proximal domain in MXRA8 (Figure 6A). Notably, MXRA8 D1 penetrates deeply into the "canyon" of the CHIKV spike in our complex structure. We propose that the 48-residue-long stalk region is sufficiently long and flexible to allow the virus spike protein to bind in such a manner, and to play a role in CHIKV entry (Figure 6B). We designed four different truncations and two different replacements (Δ48, Δ33, Δ25, Δ29, A2S, and A2T) (Figure 6A), to study the biological function of the stalk region of hMXRA8. The Δ48 and Δ33 truncations greatly affect the correct anchoring of hMXRA8 on the cell membrane, as compared with the wild type and the other truncations (Figure 6C). This indicated that the N-terminal loop of the stalk region is important for the surface expression of hMXRA8. We then used flow cytometry to test whether these truncations or replacements affected CHIKV trimeric E protein binding and infectivity. We showed that CHIKV trimeric E protein did not bind to any hMXRA8 mutant-overexpressing 293T cells, except wild type (Figure 6D). Consistent with this observation, 293T cells expressing different truncations or replacements are not infected with CHIKV (Figure 6E). These results demonstrated that the stalk region of MXRA8 is critical for CHIKV virus entry.

In conclusion, our study provides important structural insight into how CHIKV interacts with its receptor, MXRA8. MXRA8 binds in the "canyon" between two protomers of the E trimeric spike on the virion surface via multiple binding interfaces; both the Ig-like domains and the hinge region of MXRA8 are involved. Of note, the stalk region of MXRA8 is necessary for efficient binding and entry. The unique binding mode is different from those observed for other viruses, including the reovirus, coxsackie virus, adenovirus, herpes simplex virus, measles virus, and HIV-1; all of these viruses bind to the most distal domain of the Ig-like molecules (the N-terminal) (Bewley et al., 1999; Kirchner et al., 2008; Liu et al., 2017; Lu et al., 2014; Zhang et al., 2013). These findings increase our knowledge of the viral entry mechanism of enveloped viruses and may help drive the development of powerful antiviral reagents against the arthritogenic alphaviruses.

hMXRA8 wild-type protein, except for (G) R69A, (H) Y92A, and (J) R98A, for which five concentrations (5 μM, 10 μM, 20 μM, 40 μM, and 80 μM) were used for detection.

(N) SPR assay showing binding between different hMXRA8 mutant proteins and the CHIKV VLP. MXRA8 or the mutant proteins were immobilized to 3,000 response units on a CM5 chip using standard amine coupling chemistry, and CHIKV VLP was then injected at a concentration of 100 μg/mL in PBST buffer. The data were analyzed with BIAcore 3000 Evaluation software (GE Healthcare).

See also Figure S7.

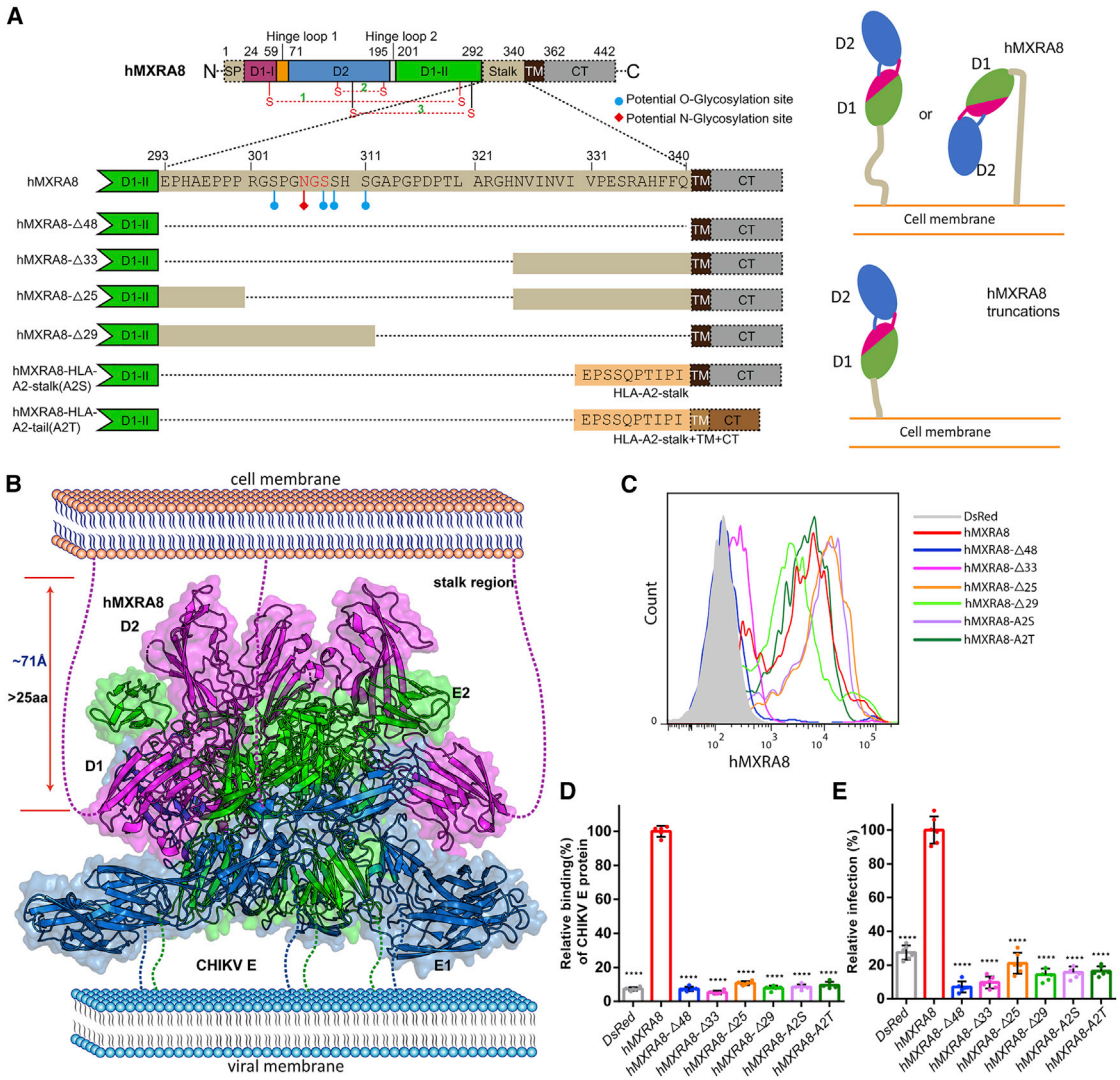

Figure 6. The Stalk Region of MXRA8 Is Critical Both for Cell Surface Expression and for CHIKV Entry

(A) Schematic overview of the hMXRA8 protein and its 48-amino acid-residue-long flexible stalk region. The amino acid sequence of the hMXRA8 stalk region from E293 to Q340 is shown. The potential N-glycosylation site and O-glycosylation sites in this region are marked with a red diamond and with blue circles, respectively. The flexibility and space conferred by the 48-amino acid-residue-long stalk region allow two different conformations to be displayed on the cell surface, where D2 is either distal or proximal to the membrane. MXRA8 mutants with truncated stalk regions can only maintain the first conformation (right panel). Different truncations, including four deletion variants (Δ48, Δ33, Δ25, and Δ29), were constructed. The deleted amino acid ranges are indicated with dots. The whole stalk region of hMXRA8 was also replaced with the stalk region of the HLA-A2 protein (named hMXRA8-HLA-A2-stalk [A2S]). Alternatively, the hMXRA8 stalk region, TM, and CT were also replaced with the corresponding parts of HLA-A2 (named hMXRA8-HLA-A2-tail [A2T]).

(B) The model of MXRA8 on the cell surface bound to the CHIKV E protein. The length of each membrane-proximal stalk of CHIKV E1, E2, or MXRA8 is indicated by dotted lines. The distances measured between the C-terminal ends to the top of MXRA8 are shown on the left, indicating the stalk region must be at least 25 aa in length in order to maintain this binding conformation.

(C) Expression levels of hMXRA8 and its different truncations on the cell surfaces of transiently transfected 293T cells were determined via flow cytometry. MXRA8 proteins were expressed by fusing with the C-terminal DsRed protein, and an anti-hMXRA8 monoclonal antibody (mAb) (MBL) was used for surface staining. Fluorescence was measured using FACSAriaIII, and DsRed-positive cells were analyzed using FlowJo 7.6.1. Results shown represent three experiments.

(D) CHIKV-E protein staining in 293T cells transiently transfected with hMXRA8 and its different truncations, as determined with flow cytometry. Cells were incubated with the CHIKV-E trimer protein fused with StrepTag II tag at a concentration of 10 μg/mL. The percentage of CHIKV-E protein staining positive cells in DsRed-positive cells were analyzed using FlowJo 7.6.1. Results show representatives of three experiments. Relative binding was normalized to wild-type MXRA8. Experiments were performed in quintuplicate, and the data are reported as mean ± SD (n = 5, multiple t tests with a Holm-Sidak correction compared to wild type). ****$p < 0.0001$.

(E) hMXRA8 and its different truncations were transiently transfected into 293T cells, which were then infected with CHIKV-181/25 at MOI 1 and stained for E2 protein. The percentage of CHIKV E2-positive cells in DsRed-positive cells was determined with FlowJo 7.6.1. Results represent three experiments. Relative infection was normalized to wild-type MXRA8. Experiments were performed in sextuplicate, and the data are reported as mean ± SD (n = 6, multiple t tests with a Holm-Sidak correction compared to wild type). ****$p < 0.0001$.

STAR★METHODS

Detailed methods are provided in the online version of this paper and include the following:

- KEY RESOURCES TABLE
- CONTACT FOR REAGENT AND RESOURCE SHARING
- EXPERIMENTAL MODEL AND SUBJECT DETAILS
  - Cells and virus
- METHOD DETAILS
  - Gene cloning, expression and protein purification
  - Crystallization, data collection and structure determination
  - Expression and purification of CHIKV virus-like particles (VLP)
  - Cryo-EM sample preparation and data collection
  - Image Processing
  - Model fitting
  - Surface staining of MXRA8 mutants
  - Cell-based CHIKV-E protein binding assay
  - Viral infection assay
  - SPR analysis
  - Biochemical characterization of MXRA8 proteins
- QUANTIFICATION AND STATISTICAL ANALYSIS
  - Binding studies
  - Flow cytometry analysis
- DATA AND SOFTWARE AVAILABILITY

SUPPLEMENTAL INFORMATION

Supplemental Information can be found online at https://doi.org/10.1016/j.cell.2019.04.008.

ACKNOWLEDGMENTS

We thank the staff of BL17U and BL19U beamlines at Shanghai Synchrotron Radiation Facility. We thank all the staff at the Center of Biological Imaging, Institute of Biophysics, Chinese Academy of Sciences (CAS), Beijing for assistance with data collection. We are grateful to Yuanyuan Chen, Bingxue Zhou, and Zhenwei Yang from Institute of Biophysics CAS for technical assistance with SPR experiments. We thank Qian Wang (Institute of Microbiology CAS) for help with analytical ultracentrifugation experiment and Tong Zhao (Institute of Microbiology CAS) for technical support for FACS experiment. This work was supported by the National Key Research and Development Program of China (2016YFD0500305 to J.Q.), the Strategic Priority Research Program of CAS (XDB29010000 to G.F.G.), the China National Grand S&T Special Project (2018ZX10101004 and 2015ZX09102024 to G.F.G.), the National Natural Science Foundation of China (NSFC) (31872745 to F.G.), the National Science and Technology Major Project (2018ZX09711003 to J.Y. and 2018ZX10733403 to H.S.), the Young Elite Scientist Sponsorship Program of China Association for Science & Technology (CAST) (2016QNRC001 to H.S.), the Youth Innovation Promotion Association CAS (2017117 to H.S.), the Excellent Young Scientist Program from NSFC (81622031 to Y.S.), and the Excellent Young Scientist Program of CAS and the Youth Innovation Promotion Association CAS (2015078 to Y.S.). G.F.G. is supported partly as a leading principal investigator of the NSFC Innovative Research Group (81621091) and the External Cooperation Program of CAS (153211KYSB20160001).

AUTHOR CONTRIBUTIONS

H.S., Y.S., J.Q., F.G., and G.F.G. designed and directed the experiments. H.S., Z.Z., X.J., C.L., F.Y., S.L., Z.G., H.W., J.S., L.V., and Y.Z. conducted the experiments. Y.C., J.Q., and F.G. collected the data-sets and solved the crystal structures. F.Y., X.J., and S.L. prepared samples for cryo-EM and S.L. collected and processed the data. H.S. Y.S., and G.F.G. analyzed the data and wrote the manuscript. Z.Z., S.T., C.M.M., J.Y., J.Q., F.G., and G.F.G. participated in the manuscript editing and discussion.

DECLARATION OF INTERESTS

The authors declare no competing interests.

Received: October 15, 2018
Revised: February 7, 2019
Accepted: April 1, 2019
Published: May 9, 2019

REFERENCES

Adams, P.D., Afonine, P.V., Bunkóczi, G., Chen, V.B., Davis, I.W., Echols, N., Headd, J.J., Hung, L.W., Kapral, G.J., Grosse-Kunstleve, R.W., et al. (2010). PHENIX: a comprehensive Python-based system for macromolecular structure solution. Acta Crystallogr. D Biol. Crystallogr. *66*, 213–221.

Arias-Goeta, C., Mousson, L., Rougeon, F., and Failloux, A.B. (2013). Dissemination and transmission of the E1-226V variant of chikungunya virus in Aedes albopictus are controlled at the midgut barrier level. PLoS ONE *8*, e57548.

Barton, E.S., Forrest, J.C., Connolly, J.L., Chappell, J.D., Liu, Y., Schnell, F.J., Nusrat, A., Parkos, C.A., and Dermody, T.S. (2001). Junction adhesion molecule is a receptor for reovirus. Cell *104*, 441–451.

Bewley, M.C., Springer, K., Zhang, Y.B., Freimuth, P., and Flanagan, J.M. (1999). Structural analysis of the mechanism of adenovirus binding to its human cellular receptor, CAR. Science *286*, 1579–1583.

Chen, W., Foo, S.S., Sims, N.A., Herrero, L.J., Walsh, N.C., and Mahalingam, S. (2015). Arthritogenic alphaviruses: new insights into arthritis and bone pathology. Trends Microbiol. *23*, 35–43.

Emsley, P., and Cowtan, K. (2004). Coot: model-building tools for molecular graphics. Acta Crystallogr. D Biol. Crystallogr. *60*, 2126–2132.

Fox, J.M., Long, F., Edeling, M.A., Lin, H., van Duijl-Richter, M.K.S., Fong, R.H., Kahle, K.M., Smit, J.M., Jin, J., Simmons, G., et al. (2015). Broadly neutralizing alphavirus antibodies bind an epitope on E2 and inhibit entry and egress. Cell *163*, 1095–1107.

Gao, G.F. (2018). From "A"IV to "Z"IKV: Attacks from Emerging and Re-emerging Pathogens. Cell *172*, 1157–1159.

Geraghty, R.J., Krummenacher, C., Cohen, G.H., Eisenberg, R.J., and Spear, P.G. (1998). Entry of alphaherpesviruses mediated by poliovirus receptor-related protein 1 and poliovirus receptor. Science *280*, 1618–1620.

Gérardin, P., Freitas, A.R.R., and Sissoko, D. (2018). Seroprevalence of Chikungunya Virus after Its Emergence in Brazil. Emerg. Infect. Dis. *24*, 1773.

Holm, L., and Rosenström, P. (2010). Dali server: conservation mapping in 3D. Nucleic Acids Res. *38*, W545-9.

Jung, Y.K., Jin, J.S., Jeong, J.H., Kim, H.N., Park, N.R., and Choi, J.Y. (2008). DICAM, a novel dual immunoglobulin domain containing cell adhesion molecule interacts with alphavbeta3 integrin. J. Cell. Physiol. *216*, 603–614.

Jung, Y.K., Han, S.W., Kim, G.W., Jeong, J.H., Kim, H.J., and Choi, J.Y. (2012). DICAM inhibits osteoclast differentiation through attenuation of the integrin αVβ3 pathway. J. Bone Miner. Res. *27*, 2024–2034.

Kirby, I., Davison, E., Beavil, A.J., Soh, C.P., Wickham, T.J., Roelvink, P.W., Kovesdi, I., Sutton, B.J., and Santis, G. (2000). Identification of contact residues and definition of the CAR-binding site of adenovirus type 5 fiber protein. J. Virol. *74*, 2804–2813.

Kirchner, E., Guglielmi, K.M., Strauss, H.M., Dermody, T.S., and Stehle, T. (2008). Structure of reovirus sigma1 in complex with its receptor junctional adhesion molecule-A. PLoS Pathog. *4*, e1000235.

Lescar, J., Roussel, A., Wien, M.W., Navaza, J., Fuller, S.D., Wengler, G., Wengler, G., and Rey, F.A. (2001). The Fusion glycoprotein shell of Semliki Forest virus: an icosahedral assembly primed for fusogenic activation at endosomal pH. Cell *105*, 137–148.

Li, H., Zhou, M., Han, J., Zhu, X., Dong, T., Gao, G.F., and Tien, P. (2005). Generation of murine CTL by a hepatitis B virus-specific peptide and evaluation of the adjuvant effect of heat shock protein glycoprotein 96 and its terminal fragments. J. Immunol. *174*, 195–204.

Li, L., Jose, J., Xiang, Y., Kuhn, R.J., and Rossmann, M.G. (2010). Structural changes of envelope proteins during alphavirus fusion. Nature *468*, 705–708.

Li, X., Mooney, P., Zheng, S., Booth, C.R., Braunfeld, M.B., Gubbens, S., Agard, D.A., and Cheng, Y. (2013). Electron counting and beam-induced motion correction enable near-atomic-resolution single-particle cryo-EM. Nat. Methods *10*, 584–590.

Liu, Q., Acharya, P., Dolan, M.A., Zhang, P., Guzzo, C., Lu, J., Kwon, A., Gururani, D., Miao, H., Bylund, T., et al. (2017). Quaternary contact in the initial interaction of CD4 with the HIV-1 envelope trimer. Nat. Struct. Mol. Biol. *24*, 370–378.

Long, F., Fong, R.H., Austin, S.K., Chen, Z., Klose, T., Fokine, A., Liu, Y., Porta, J., Sapparapu, G., Akahata, W., et al. (2015). Cryo-EM structures elucidate neutralizing mechanisms of anti-chikungunya human monoclonal antibodies with therapeutic activity. Proc. Natl. Acad. Sci. USA *112*, 13898–13903.

Lu, G., Zhang, N., Qi, J., Li, Y., Chen, Z., Zheng, C., Gao, G.F., and Yan, J. (2014). Crystal structure of herpes simplex virus 2 gD bound to nectin-1 reveals a conserved mode of receptor recognition. J. Virol. *88*, 13678–13688.

Mainou, B.A., Zamora, P.F., Ashbrook, A.W., Dorset, D.C., Kim, K.S., and Dermody, T.S. (2013). Reovirus cell entry requires functional microtubules. MBio *4*, e00405-13.

Mastronarde, D.N. (2005). Automated electron microscope tomography using robust prediction of specimen movements. J. Struct. Biol. *152*, 36–51.

Mejía, C.R., and López-Vélez, R. (2018). Tropical arthritogenic alphaviruses. Reumatol. Clin. *14*, 97–105.

Otwinowski, Z., and Minor, W. (1997). Processing of X-ray diffraction data collected in oscillation mode. Methods Enzymol. *276*, 307–326.

Pal, P., Dowd, K.A., Brien, J.D., Edeling, M.A., Gorlatov, S., Johnson, S., Lee, I., Akahata, W., Nabel, G.J., Richter, M.K., et al. (2013). Development of a highly protective combination monoclonal antibody therapy against Chikungunya virus. PLoS Pathog. *9*, e1003312.

Pettersen, E.F., Goddard, T.D., Huang, C.C., Couch, G.S., Greenblatt, D.M., Meng, E.C., and Ferrin, T.E. (2004). UCSF Chimera–a visualization system for exploratory research and analysis. J. Comput. Chem. *25*, 1605–1612.

Read, R.J. (2001). Pushing the boundaries of molecular replacement with maximum likelihood. Acta Crystallogr. D Biol. Crystallogr. *57*, 1373–1382.

Robert, X., and Gouet, P. (2014). Deciphering key features in protein structures with the new ENDscript server. Nucleic Acids Res. *42*, W320-4.

Rohou, A., and Grigorieff, N. (2015). CTFFIND4: Fast and accurate defocus estimation from electron micrographs. J. Struct. Biol. *192*, 216–221.

Ronca, S.E., Dineley, K.T., and Paessler, S. (2016). Neurological Sequelae Resulting from Encephalitic Alphavirus Infection. Front. Microbiol. *7*, 959.

Scheres, S.H. (2012). RELION: implementation of a Bayesian approach to cryo-EM structure determination. J. Struct. Biol. *180*, 519–530.

Smith, S.A., Silva, L.A., Fox, J.M., Flyak, A.I., Kose, N., Sapparapu, G., Khomandiak, S., Ashbrook, A.W., Kahle, K.M., Fong, R.H., et al. (2015). Isolation and characterization of broad and ultrapotent human monoclonal antibodies with therapeutic activity against Chikungunya virus. Cell Host Microbe *18*, 86–95.

Song, H., Qi, J., Haywood, J., Shi, Y., and Gao, G.F. (2016). Zika virus NS1 structure reveals diversity of electrostatic surfaces among flaviviruses. Nat. Struct. Mol. Biol. *23*, 456–458.

Suhrbier, A., Jaffar-Bandjee, M.C., and Gasque, P. (2012). Arthritogenic alphaviruses–an overview. Nat. Rev. Rheumatol. *8*, 420–429.

Sun, S., Xiang, Y., Akahata, W., Holdaway, H., Pal, P., Zhang, X., Diamond, M.S., Nabel, G.J., and Rossmann, M.G. (2013). Structural analyses at pseudo atomic resolution of Chikungunya virus and antibodies show mechanisms of neutralization. eLife *2*, e00435.

Tang, G., Peng, L., Baldwin, P.R., Mann, D.S., Jiang, W., Rees, I., and Ludtke, S.J. (2007). EMAN2: an extensible image processing suite for electron microscopy. J. Struct. Biol. *157*, 38–46.

Voss, J.E., Vaney, M.C., Duquerroy, S., Vonrhein, C., Girard-Blanc, C., Crublet, E., Thompson, A., Bricogne, G., and Rey, F.A. (2010). Glycoprotein organization of Chikungunya virus particles revealed by X-ray crystallography. Nature *468*, 709–712.

Williams, C.J., Headd, J.J., Moriarty, N.W., Prisant, M.G., Videau, L.L., Deis, L.N., Verma, V., Keedy, D.A., Hintze, B.J., Chen, V.B., et al. (2018). MolProbity: More and better reference data for improved all-atom structure validation. Protein Sci. *27*, 293–315.

Xu, X., Song, H., Qi, J., Liu, Y., Wang, H., Su, C., Shi, Y., and Gao, G.F. (2016). Contribution of intertwined loop to membrane association revealed by Zika virus full-length NS1 structure. EMBO J. *35*, 2170–2178.

Yap, M.L., Klose, T., Urakami, A., Hasan, S.S., Akahata, W., and Rossmann, M.G. (2017). Structural studies of Chikungunya virus maturation. Proc. Natl. Acad. Sci. USA *114*, 13703–13707.

Yonezawa, T., Ohtsuka, A., Yoshitaka, T., Hirano, S., Nomoto, H., Yamamoto, K., and Ninomiya, Y. (2003). Limitrin, a novel immunoglobulin superfamily protein localized to glia limitans formed by astrocyte endfeet. Glia *44*, 190–204.

Zanotto, P.M.A., and Leite, L.C.C. (2018). The Challenges Imposed by Dengue, Zika, and Chikungunya to Brazil. Front. Immunol. *9*, 1964.

Zhang, W., Qi, J., Shi, Y., Li, Q., Gao, F., Sun, Y., Lu, X., Lu, Q., Vavricka, C.J., Liu, D., et al. (2010). Crystal structure of the swine-origin A (H1N1)-2009 influenza A virus hemagglutinin (HA) reveals similar antigenicity to that of the 1918 pandemic virus. Protein Cell *1*, 459–467.

Zhang, N., Yan, J., Lu, G., Guo, Z., Fan, Z., Wang, J., Shi, Y., Qi, J., and Gao, G.F. (2011). Binding of herpes simplex virus glycoprotein D to nectin-1 exploits host cell adhesion. Nat. Commun. *2*, 577.

Zhang, X., Lu, G., Qi, J., Li, Y., He, Y., Xu, X., Shi, J., Zhang, C.W.H., Yan, J., and Gao, G.F. (2013). Structure of measles virus hemagglutinin bound to its epithelial receptor nectin-4. Nat. Struct. Mol. Biol. *20*, 67–72.

Zhang, R., Kim, A.S., Fox, J.M., Nair, S., Basore, K., Klimstra, W.B., Rimkunas, R., Fong, R.H., Lin, H., Poddar, S., et al. (2018). Mxra8 is a receptor for multiple arthritogenic alphaviruses. Nature *557*, 570–574.

STAR★METHODS

KEY RESOURCES TABLE

REAGENT or RESOURCE	SOURCE	IDENTIFIER
Antibodies		
StrepTag II Mouse Monoclonal antibody	Easybio	Cat# BE2076; RRID: AB_2801290
Fluorescein-Conjugated AffiniPure Goat Anti-Mouse IgG (H+L)	Zsbio	Cat# ZF-0312; RRID: AB_2716306
anti-MXRA8 (human) mAb	MBL	Cat# W040-3; RRID: AB_2801291
Bacterial and Virus Strains		
Escherichia coli (*E. coli*) strain BL21 (DE3)	Novagen	Cat# 69450
Escherichia coli (*E. coli*) strain DH5α	TIANGEN	Cat# CB101-02
MAX Efficiency DH10Bac Competent *E. coli*	Invitrogen	Cat# 10361-012
CHIKV-181/25	Mainou et al., 2013	Addgene # 60078
Chemicals, Peptides, and Recombinant Proteins		
PEI	Alfa	A04043896-1g
Sucrose	Sigma	V900116-500 g
Human MXRA8-2 isoform, GENBANK: NP_115724	This paper	N/A
Mouse MXRA8, GENBANK: NP_077225	This paper	N/A
Recombinant CHIKV p62-E1 proteins, GENBANK: ABN04188	This paper	N/A
Recombinant ONNV p62-E1 proteins, GENBANK: AF079456	This paper	N/A
Critical Commercial Assays		
HisTrap HP 5 ml column	GE Healthcare	Cat# 17524802
StrepTrap HP 5 ml column	GE Healthcare	Cat# 28907548
Superdex 75 10/300 GL	GE Healthcare	Cat# 17517401
Superdex 200 Increase 10/300 GL	GE Healthcare	Cat# 28990944
HiLoad 16/600 Superdex 75 pg	GE Healthcare	Cat# 28989333
HiLoad 16/600 Superdex 200 pg	GE Healthcare	Cat# 28989335
HiTrap Protein G HP	GE Healthcare	Cat# 17040503
Crystallization kits	Hampton Research and Molecular Dimensions	http://www.hamptonresearch.com; https://www.moleculardimensions.com/
Membrane concentrator	Millipore	UFC901096
Series S Sensor Chip CM5	GE Healthcare	Cat# 29149603
His Capture Kit	GE Healthcare	Cat# 28995056
Deposited Data		
Crystal structure of mMXRA8	This paper	PDB: 6JO7
Crystal structure of hMXRA8/CHIKV E complex	This paper	PDB: 6JO8
Cryo-EM hMXRA8/CHIKV VLP complex	This paper	EM Data Bank: EMD-9857
Experimental Models: Cell Lines		
Sf9 Cells, SFM Adapted	Invitrogen	Cat# 11496015
High Five cells	Invitrogen	Cat# B85502
293T cells	ATCC	ATCC CRL-3216
Vero cells	ATCC	ATCC CCL-81
Recombinant DNA		
pET-21a(+)	Novagen	Cat# 69740
pET-21a(+)-hMXRA8, mMXRA8, various mutants	This paper	N/A

(*Continued on next page*)

Continued

REAGENT or RESOURCE	SOURCE	IDENTIFIER
pFastbac Dual	Invitrogen	Cat# 10712024
pFastbac Dual-CHIKV-p62-E1	This paper	N/A
pFastbac Dual-ONNV-p62-E1	This paper	N/A
pLVX-DsRed-Monomer-N1	Clonetech	Cat# 632152
pLVX-DsRed-Monomer-N1-hMXRA8, various mutants	This paper	N/A
pCAGGS-CHIKV-C-E (strain 11906, Accession codes: APA34057)	This paper	N/A
pCAGGS-CHK-265-L	This paper	N/A
pCAGGS-CHK-265-H	This paper	N/A
Software and Algorithms		
PyMOL software	Molecular Graphics System, Version 1.8 Schrö dinger	https://pymol.org/2/
BIAcore® T100 Evaluation software, version 2.0.1	GE Healthcare	N/A
BIAcore® 3000 Evaluation software	GE Healthcare	N/A
Graphpad Prism 6	GraphPad Software	https://www.graphpad.com/
Flowjo 7.6.1	FLOWJO	https://www.flowjo.com/solutions/flowjo/downloads
HKL2000	Otwinowski and Minor, 1997	N/A
Phaser	Read, 2001	N/A
COOT	Emsley and Cowtan, 2004	https://www2.mrc-lmb.cam.ac.uk/personal/pemsley/coot/
Phenix	Adams et al., 2010	http://www.phenix-online.org/
MolProbity	Williams et al., 2018	N/A
ESPript 3	Robert and Gouet, 2014	http://espript.ibcp.fr/ESPript/ESPript/
MOTIONCORR	Li et al., 2013	N/A
e2boxer.py	Tang et al., 2007	N/A
CTFFIND4	Rohou and Grigorieff, 2015	N/A
Relion-1.4	Scheres, 2012	N/A
SerialEM	Mastronarde, 2005	N/A

CONTACT FOR REAGENT AND RESOURCE SHARING

Further information and requests for resources and reagents should be directed to and will be fulfilled by the Lead Contact, George F. Gao (gaof@im.ac.cn).

EXPERIMENTAL MODEL AND SUBJECT DETAILS

Cells and virus

Vero (ATCC CCL-81), HEK293T (ATCC CRL-3216) cells were cultured at 37°C in Dulbecco's Modified Eagle medium (DMEM) supplemented with 10% fetal bovine serum (FBS). CHIKV-181/25 strain (Mainou et al., 2013) was propagated in Vero cells and titrated by standard plaque assays.

METHOD DETAILS

Gene cloning, expression and protein purification

The DNA encoding the Ig-like domain of mMXRA8 (residues S22–T291, Genbank: NP_077225) and the human MXRA8-2 isoform (hMXRA8, residues G25–A292, Genbank: NP_115724) were separately cloned into the *p*ET21a vector (Novagen) with *Nde*I and *Xho*I restriction sites and transformed into *Escherichia coli* (*E. coli*) strain BL21 (DE3) for protein expression. The predicted hMXRA8-pD1 (residues G25–G159) and hMXRA8-pD2 (residues P160–A292) plasmids were constructed in the same way. The inclusion bodies of the recombinant proteins were purified and refolded as described, with some modifications (Li et al., 2005; Song et al., 2016). Briefly, aliquots of inclusion bodies were diluted dropwise in an agitating refolding buffer (100 mM Tris-HCl,

2 mM EDTA, 400 mM L-arginine, 0.5 mM oxidized glutathione and 5 mM reduced glutathione, pH 8.0) for 8 h at 4°C. The refolded protein was concentrated and buffer-exchanged using an Amicon® 8400 concentrator to the solution containing 20 mM Tris-HCl and 150 mM NaCl, pH 8.0. Subsequently, the proteins were further purified by gel-filtration chromatography in the same exchange buffer aforementioned on a HiLoad® 16/600 Superdex® 75 pg column (GE Healthcare). The eligible peak fractionated proteins were concentrated for further study or crystallization. The mutant hMXRA8 plasmids were constructed by site-directed mutagenesis, for which the identified residues involved in CHIKV E3-E2-E1 binding were mutated separately (Q63A; D64A; R69A; Y92A; E96A; R98A; E227A/R228A; C144A/C279A; C144S/C279S).

We produced the recombinant p62-E1 proteins with the Bac-to-Bac baculovirus expression system (Invitrogen) (Zhang et al., 2010). The coding sequences for CHIKV p62-E1 (GenBank: ABN04188), ONNV p62-E1 (GenBank: AF079456) were individually cloned into a modified *p*Fastbac Dual Plasmid (Invitrogen) under the control of polyhedrin promoter (Xu et al., 2016). We placed green fluorescent protein (GFP) under the control of P10 promoter to visualize its expression. A 20-residue linker, of sequence $(GGGGS)_4$ connected the C terminus of the p62 ectodomain to the N terminus of E1, thus bypassing the p62 transmembrane region and the 6K protein. The actual construct contained amino acids 1–405 of p62 (the last one corresponding to E2 residue 341) and 1–412 of E1 (that is, all of the ectodomain, stopping right at the beginning of the transmembrane segment of E1). For each construct, the separately-authentic p62 signal sequence was used, and the Twin-Strep-tag® II was placed in front of the hexa-His tag were added to the C terminus to facilitate further purification processes. Recombinant *p*Fastbac Dual plasmids were used to transform DH10Bac™ *E. coli* (Invitrogen). Transfection and virus amplification were conducted with sf9 cells, and the recombinant proteins were expressed in High Five cells (Invitrogen) for 2 days. The secreted proteins were the mature E3-E2-E1 complexes, resulting from maturation of p62 by presumably-furin-like enzyme. Soluble E proteins were recovered from cell supernatants by metal affinity chromatography using a HisTrap HP 5 mL column (GE Healthcare) and then purified by another round of affinity chromatography using a StrepTrap HP 5 mL column (GE Healthcare). For crystallization, the proteins were further purified by gel-filtration chromatography using a HiLoad® 16/600 Superdex® 200 pg column (GE Healthcare) with a running buffer of 20 mM Tris-HCl and 150 mM NaCl (pH 8.0).

Full-length cDNA of the heavy chain and light chain of CHK-265 antibody (Pal et al., 2013; Fox et al., 2015) were synthesized and inserted into the pCAGGS vector respectively for generation of IgG and then expressed in 293T cells and purified by conventional methods. Soluble IgG was harvested from the culture supernatants by Protein G affinity chromatography (GE Healthcare) and subsequently purified by gel filtration on a HiLoad® 16/600 Superdex® 200 pg column (GE Healthcare) in PBS buffer.

Crystallization, data collection and structure determination

Crystallization trials were set up with commercial crystallization kits (Hampton Research and Molecular Dimensions) using the sitting-drop vapor-diffusion method. Normally, 0.8 μL protein with corresponding concentrations was mixed with 0.8 μL reservoir solution. The resultant drop was then sealed, equilibrating against 90 μL reservoir solution at 4 or 18°C. Diffractable crystals of mMXRA8 were obtained in 0.1 M BICINE pH 8.5, 15% w/v Polyethylene glycol 1,500 at 18°C. The MXRA8 and CHIKV E3-E2-E1 complex was prepared by mixing in a 1:1 or 2:1 molar ratio and incubated on ice for 5 hours before concentrated to 10 mg/ml using a membrane concentrator with a molecular weight cutoff of 10 kDa (Millipore). The mixture was then directly set up the crystallization trials. High quality MXRA8 and CHIKV E3-E2-E1 complex crystals were obtained in 1M Ammomium phophate dibasic, 0.1M sodium acetate pH 4.5 with a protein concentration of 10 mg/ml. The complex crystals were further optimized and higher levels of diffraction were finally obtained under the condition containing 0.8M Ammomium phophate dibasic, 0.1M sodium acetate pH 6.0.

Crystals were flash-cooled in liquid nitrogen after a brief soak in reservoir solution with the addition of 20% (v/v) glycerol. X-ray diffraction data were collected under cryogenic conditions (100K) at Shanghai Synchrotron Radiation Facility (SSRF). The mMXRA8 datasets were collected at BL17U1, while the hMXRA8 and CHIKV E3-E2-E1 complex datasets were collected at BL19U1. The data were indexed, integrated, and scaled with HKL2000 (Otwinowski and Minor, 1997). The structures of mMXRA8 was determined by the molecular replacement method using Phaser (Read, 2001) with an Ig like molecule (PDB : 3TT3). The final dataset of hMXRA8 and CHIKV E3-E2-E1 used for structure determination were merged by nine individual crystal diffraction datasets. The complex structure was further determined by the refined mMXRA8 structure and the previously reported CHIKV E structure (PDB: 3N40). The atomic models were completed with COOT (Emsley and Cowtan, 2004) and refined with phenix.refine in Phenix (Adams et al., 2010), and the stereochemical qualities of the final models were assessed with MolProbity (Williams et al., 2018). Data collection, processing, and refinement statistics are summarized in Table S1. All structural figures were generated using PyMOL software (https://pymol.org/2/).

Expression and purification of CHIKV virus-like particles (VLP)

The full-length genes encoding the CHIKV capsid protein and enveloped protein (strain 119067; GenBank: APA34057) were synthesized and cloned into the pCAGGS plasmid. The VLP expression plasmid was then transfected into 293T cells. At 72 hours post transfection, the supernatant was collected and centrifuged at 10,000 × g for 1 h to remove cells and other debris. Initial purification was carried out by ultracentrifugation through a 30% (w/v) sucrose cushion using a type 45Ti rotor at 80,000 g for 1 h at 4°C. The crude virus was resuspended in PBS (phosphate buffered saline; pH 7.4), and loaded into a discontinuous sucrose gradient (20%–60% w/v) for further purification via centrifugation, using a Beckmann SW41 rotor at 100,000 × g at 4°C for 8 h. The fractions containing the CHIKV VLP were collected and concentrated in PBS. The virus band was extracted from the gradient using a syringe.

The sample was then buffer-exchanged to PBS buffer and concentrated using an Amicon Ultra-6 100 kDa cutoff centrifugal concentrator (Millipore).

Cryo-EM sample preparation and data collection

To obtain the CHIKV VLP and MXRA8 complex, the excess MXRA8 was incubated with purified CHIKV VLP at 4°C for 6 hours before freezing. For Cryo-EM specimen preparation, 4 μL of the CHIKV VLP-MXRA8 complex was transferred onto a glow-discharged ultrathin carbon-coated copper grid, allowed to stand for 60 s, blotted for 3 s with filter paper, and plunged into liquid ethane using the FEI Vitrobot Mark IV. Cryo-EM datasets were collected at 300 kV with a Titan Krios microscope (FEI), equipped with a direct electron detector (K2 Summit, Gatan). Movies (32 frames, total dose 40e $Å^{-2}$) were recorded with a defocus between −1.0 and −3.0 μm in super-resolution counting mode using SerialEM (Mastronarde, 2005) at a calibrated magnification of 37,027 ×, resulting in a pixel size of 1.35 Å.

Image Processing

Micrographs were corrected for beam-induced drift using MOTIONCORR (Li et al., 2013). We manually selected 28,997 particles from 2904 micrographs using e2boxer.py (Tang et al., 2007). The initial contrast transfer function (CTF) parameters were estimated with CTFFIND4 (Rohou and Grigorieff, 2015). All of the subsequent image processing and reconstruction steps were handled in Relion-1.4 (Scheres, 2012). Briefly, images with a binning factor of 4 were pooled for 2D classification to remove the heterogeneous particles, which yielded poor 2D class average images. A clean dataset with 10,988 particles from good 2D classes was selected and subjected to further 3D classification using the Cryo-EM map of CHIKV VLP (EM Data Bank: EMD-5577), low-pass filtered to 60 Å as the initial model. Among the four 3D classes, a predominant class showed the best structural features and the highest accuracy of particle alignment. This class contained a subset of 1,596 best particles. The coordinates for these particles were exported in order to extract the full-size images for final reconstruction. The resulting map had a resolution of 8.9 Å, as shown by a Fourier shell correlation curve, with a cutoff value of 0.143 (Figure S2).

Model fitting

The Cryo-EM structure of CHIKV VLP (EM Data Bank: EMD-5577) was initially fitted into the resulting density map with Chimera (Pettersen et al., 2004); the structure was well correlated with the map. Subsequently, the atomic structure of the hMXRA8-CHIKV E1-E2 complex was further fitted into the map, and showed a high degree of matching. The E3 protein was not apparent in the cryoEM density map, consistent with previously described CHIKV VLP cryoEM structures (Sun et al., 2013).

Surface staining of MXRA8 mutants

The DNA encoding the full-length human MXRA8-2 isoform (Genbank: AB052096) was cloned into the pLVX-DsRed-Monomer-N1 (Clonetech), with EcoRI and BamHI restriction sites, to express the MXRA8 protein fused with the C-terminal DsRed protein. Six different stalk region truncation mutants [hMXRA8-Δ25, hMXRA8-Δ29, hMXRA8-Δ33, hMXRA8-Δ48, hMXRA8-HLA-A2-stalk (A2S), and hMXRA8-HLA-A2-tail (A2T)] were separately constructed using the overlapping PCR method, cloned into the pLVX-DsRed-Monomer-N1 plasmid, and transformed into *E. coli* strain DH5α for amplification.

We plated 2 × 10^5 cells per well in a 24-well plate 24 h before the experiment. Then, 293T cells were transiently transfected with plasmids of hMXRA8 or its mutants for surface staining. At 48 h post-transfection, cells were collected and stained with 2 μg/ml anti-hMXRA8 mAb (MBL) for 30 minutes. After washing twice with PBS, anti-mIgG/FITC (Zsbio) was added and incubated for 30 minutes. Fluorescence was measured using FACSAriaIII and analyzed using FlowJo 7.6.1 (https://www.flowjo.com/).

Cell-based CHIKV-E protein binding assay

We used 293T cells, transiently transfected with plasmids of hMXRA8 and its mutants, for the binding test. At 48 h post-transfection, cells were collected and incubated with 10 μg/mL of the CHIKV-E trimer protein fused with the StrepTag II tag for 30 minutes. After washing twice with PBS, mouse-derived StrepTag II mab (Bioeasytech) was added and incubated for 30 minutes. After washing twice, anti-mIgG/FITC (Zsbio) was added and incubated for 30 minutes. After washing, fluorescence was measured using FACSAriaIII. The percentage of CHIKV-E protein staining positive cells in DsRed-positive cells were analyzed using FlowJo 7.6.1. The column chart was generated with GraphPad Prism6.

Viral infection assay

We plated 2 × 10^5 cells per well in a 24-well plate 24 h before conducting the experiment. Then, 293T cells were transiently transfected with plasmids of hMXRA8 and its mutants. At 48 h post-transfection, cells were incubated with CHIKV-181/25 at MOI 1. After 1 h of adsorption, 500 μL of DMEM with 2% fetal bovine serum was exchanged in each well, and cells were cultured for 9.5 h. Next, infected cells were collected using trypsin, then fixed and permeabilized using fixation and permeabilization solution (BD Biosciences) at 4°C for 30 minutes. Cells were then stained with 5 μg/mL CHK-265 antibody diluted with PBS (Pal et al., 2013) at 4°C for another 30 minutes. Cells were washed twice with 1 × Perm/Wash buffer (BD Biosciences) and then stained with anti-mIgG/FITC

(Zsbio), diluted 1:200 in PBS, at 4°C for 30 minutes. After washing, fluorescence was measured using FACSAriaIII. The percentage of CHIKV E2 positive cells in DsRed-positive cells were analyzed using FlowJo 7.6.1 and the column chart was generated using GraphPad Prism6.

SPR analysis

The SPR analysis of affinity between CHIKV-E and MXRA8 was performed using a BIAcore T100 with CM5 chips (GE Healthcare) linked with anti-his antibody at 25°C. All of the proteins used for SPR analysis were buffer-exchanged to PBST (10 mM Na_2HPO_4; 2mM KH_2PO_4, pH 7.4; 137 mM NaCl; 2.7 mM KCl; 0.005% Tween 20). CHIKV-E monomer and trimer proteins were separately captured by the anti-his antibody. The MXRA8 proteins were serially diluted. hMXRA8, mMXRA8, hMXRA8-Q63A, hMXRA8-D64A, hMXRA8-E96A, hMXRA8-E227A/R228A, hMXRA8-C144A/C279A, and hMXRA8-C144S/C279S were injected at concentrations of 1.25, 2.5, 5, 10, and 20 μM. hMXRA8-R69A, hMXRA8-Y92A, and hMXRA8-R98A were loaded at concentrations of 5, 10, 20, 40, and 80 μM. The analytes were then used to flow over the chip surface, with the response units measured at single cycle. The binding kinetics were analyzed using 1:1 binding model with BIAcore T100 Evaluation software, version 2.0.1 (GE Healthcare). No obvious binding differences between the CHIKV-E monomer and trimer proteins were observed.

The interactions between MXRA8 or its mutants and CHIKV VLP were measured using a BIAcore T100. MXRA8 or its mutant proteins were immobilized to 3000 response units on a CM5 chip using standard amine coupling chemistry. We then injected 100 μg/ml CHIKV VLP in PBST. The data were analyzed with BIAcore 3000 Evaluation (GE Healthcare).

Biochemical characterization of MXRA8 proteins

The purified MXRA8 proteins were analyzed with an analytical gel-filtration assay with a calibrated Superdex® 75 10/300 GL column (GE Healthcare). The samples were further analyzed with SDS-PAGE.

Analytical ultracentrifugation experiments were performed in a Beckman Optima XL-I, using an AN-50 Ti rotor with two-channel charcoal-filled centerpieces at 4°C or 20°C. The proteins were prepared in a buffer containing 20 mM Tris-HCl and 150 mM NaCl, pH 8.0 at a concentration of A_{280} = 0.8. Absorbance data were acquired at a wavelength of 280 or 230 nm, respectively. The molecular mass analysis was performed with the XL-I data analysis software.

QUANTIFICATION AND STATISTICAL ANALYSIS

Binding studies

KD values for SPR experiments were obtained with BIAcore T100 Evaluation software, version 2.0.1 (GE Healthcare), using a 1:1 binding model. The values shown are the mean ± SEM of three independent experiments.

Flow cytometry analysis

All of the experiments were performed three times; one representative of each experiment is shown in Figure 5. For the CHIKV-E protein staining or CHIKV infection assays, experiments were performed five or six times, and the data are reported as mean ± SD. Relative binding or infection was normalized to wild-type MXRA8, and we considered differences statistically significance when P values were < 0.05 according to multiple t tests with a Holm–Sidak correction in GraphPad Prism 6.

DATA AND SOFTWARE AVAILABILITY

The accession numbers for the atomic coordinates and diffraction data reported in this paper are PDB: 6JO7 (crystal structure of mMXRA8) and PDB: 6JO8 (crystal structure of hMXRA8/CHIKV E complex).

The accession number for the cryo-EM density maps reported in this paper are EM Data Bank: EMD-9857 (hMXRA8/CHIKV VLP complex).

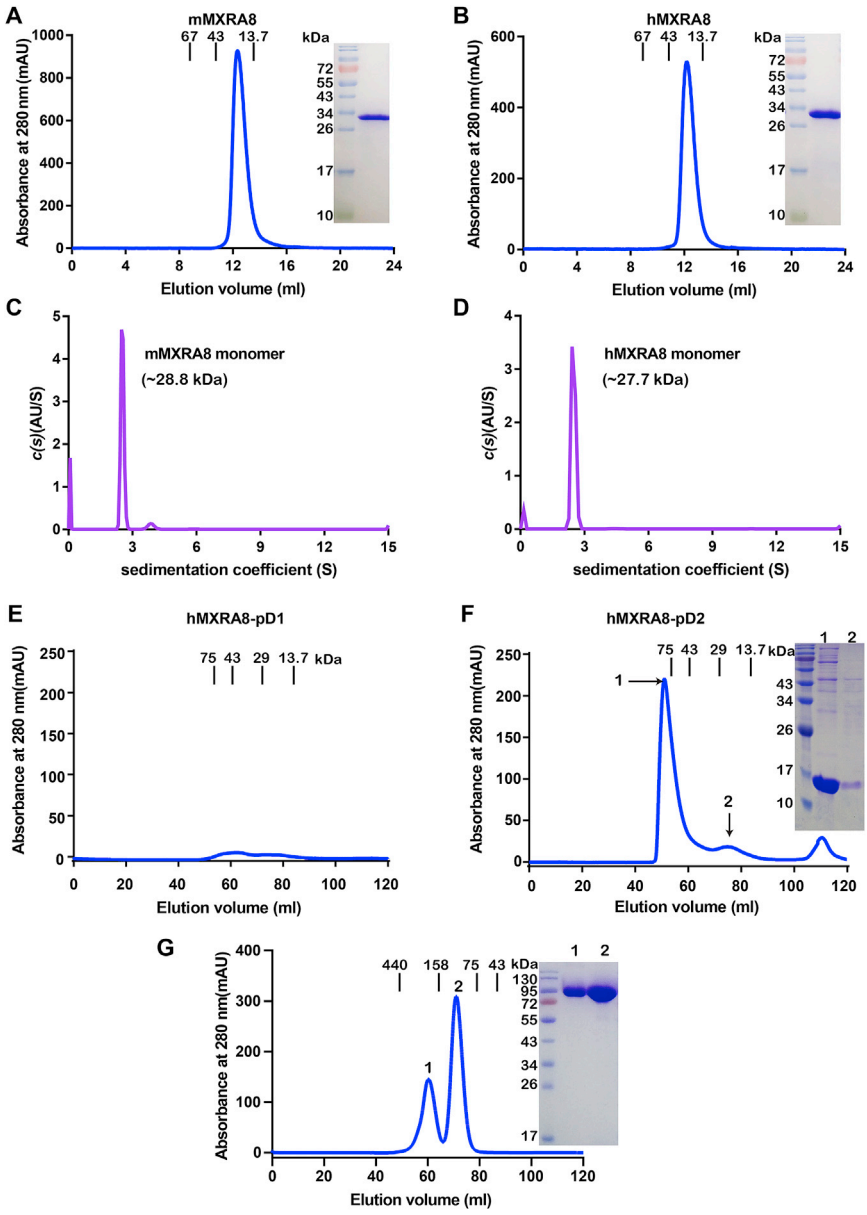

Figure S1. Biophysical Characterization of the mMXRA8, hMXRA8, and CHIKV E Proteins, Related to Figure 1

Analytical gel filtration of mMXRA8 (A) and hMXRA8 (B) proteins with Superdex® 75 10/300 GL. The 280-nm absorbance curve and the SDS-PAGE migration profile of the pooled sample are shown. Predicted monomeric molecules are seen. Ultracentrifugation sedimentation profiles of mMXRA8 (C) and hMXRA8 (D). The calculated molecular weight of the indicated protein species is shown, monomer. Analytical gel filtration of predicted D1 domain (G25-G159, hMXRA8-pD1) (E) and D2 domain (P160-A292, hMXRA8-pD2) (F) refolding efficiency with HiLoad® 16/600 Superdex® 75 pg, indicating no refolding for pD1 and inefficient refolding for pD2, implying the special folds. The 280-nm absorbance curve and the SDS-PAGE migration profile of the pooled sample are shown. (G) Analytical gel filtration profile of CHIKV E proteins with HiLoad® 16/600 Superdex® 200 pg. The 280-nm absorbance curve and the SDS-PAGE migration profile of the pooled sample are shown. Both the monomeric and trimeric E molecules are seen in solution.

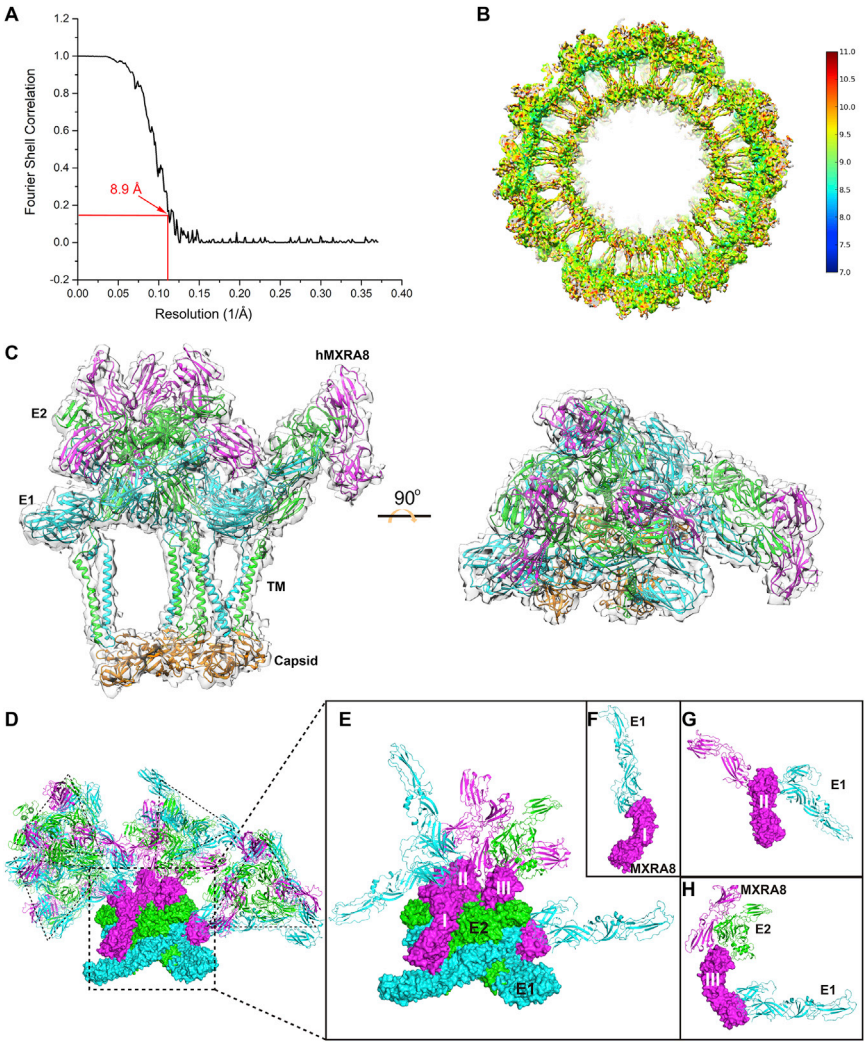

Figure S2. The Cryo-EM Complex Structure of CHIKV VLP Bound to hMXRA8 Supports the Binding Mode Observed in Our Crystal Complex Structure, Related to Figure 2

(A) The gold standard Fourier shell correlation (FSC) curve of the final density map of the cryo-EM complex structure, (B) Resolution distribution in the cryo-EM map according to the scale provided at the right side. (C) The asymmetric unit in the cryo-EM structure shown in side view (left) and top view (right) using ribbon representation. CHIKV E1 and E2 including their transmembrane regions (TM) are shown in cyan and green respectively, CHIKV capsid in orange, and hMXRA8 in magenta. The Cryo-EM map is represented as a gray transparent surface. (D) Crystal packing of hMXRA8 and CHIKV E complex. E1 is shown in cyan, E2 in green, and hMXRA8 in magenta. The proteins in one asymmetric unit are shown in surface representation and the other molecules are shown as cartoon. The three hMXRA8 molecules (labeled I, II, III) in one asymmetric unit interact with neighboring molecules in distinct ways. (E) The molecules interacting with the three hMXRA8 are highlighted, and further binding details of hMXRA8 I (F), II (G), III (H) with corresponding neighboring molecules are shown respectively. The interactions of hMXRA8 with other molecules in the neighboring asymmetric units by crystal packing are much weaker compared to the hMXRA8 binding to the E complex, and will not influence the orientation of the MXRA8 domains.

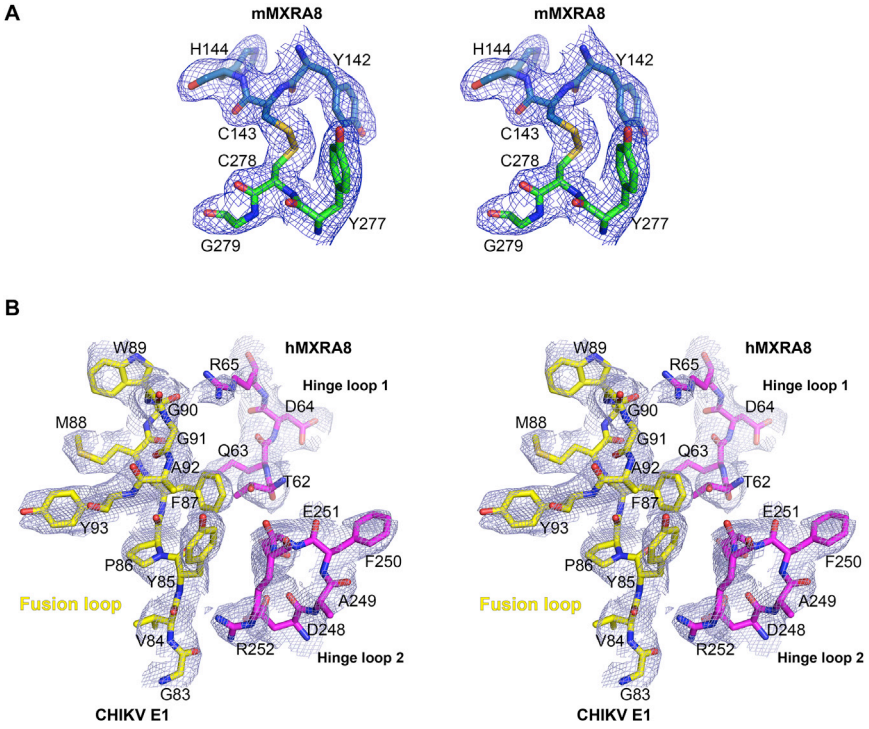

Figure S3. Stereo View of the Representative Final Electron Density Map for Structures, Related to Figures 1 and 2

(A) The final 2Fo-Fc density map of mMXRA8 is drawn in blue mesh contoured at 1 sigma. (B) The final 2Fo-Fc density map of the complex structure of CHIKV E3-E2-E1 glycoprotein bound to hMXRA8 is drawn in light blue mesh contoured at 1 sigma. This picture indicates the quality of the data at the interface between hMXRA8 and CHIKV E1 fusion loop.

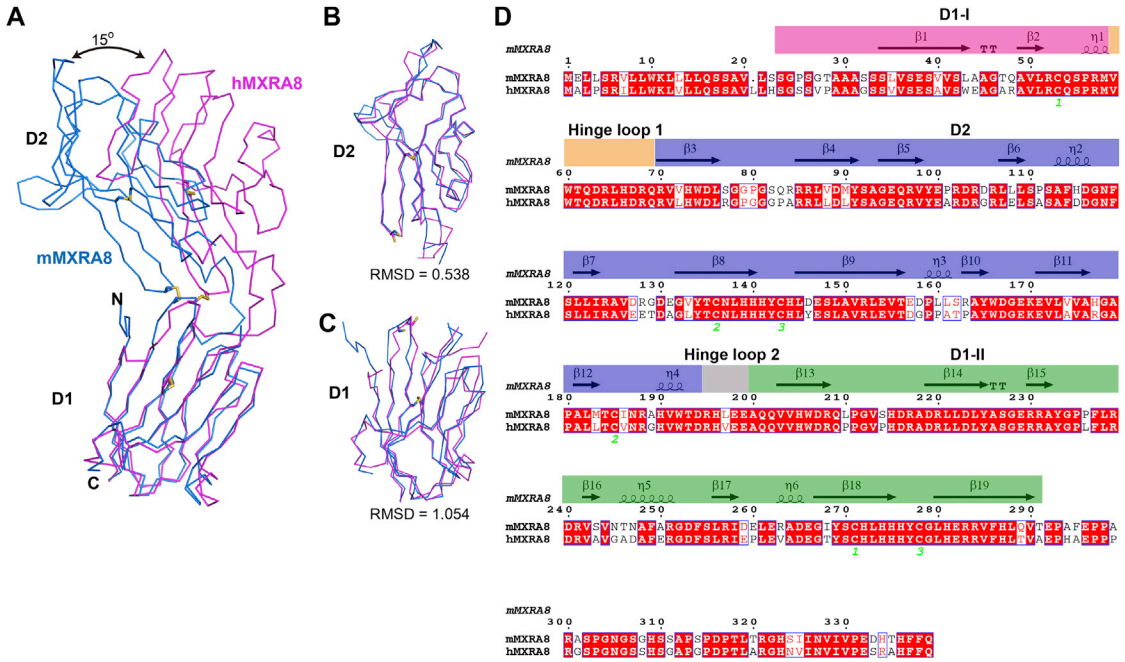

Figure S4. Structural Comparison of mMXRA8 and hMXRA8, Related to Figure 2

The interdomain angle of D1-D2 in mMXRA8 and hMXRA8 shows a 15° shift (A), although each domain maintained similar folds, with RMSD at 0.538 (B), D2) and 1.054 (C), D1). (D) Secondary structures and sequence alignment of mMXRA8 and hMXRA8 proteins. Sequence alignment was produced by ESPript (Robert and Gouet, 2014).

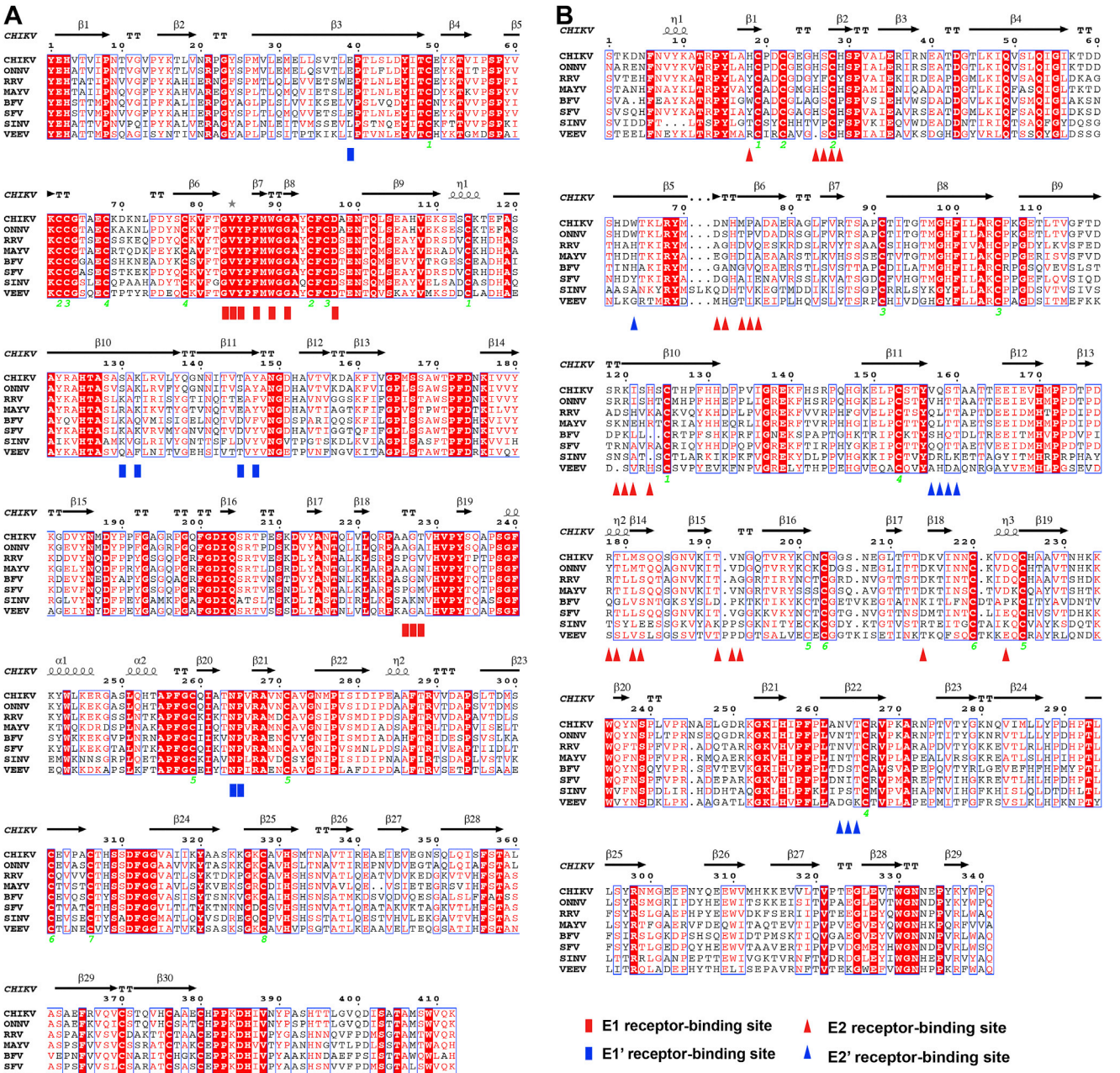

Figure S5. Sequence Alignment of E1 and E2 Proteins from Eight Representative Alphaviruses, Related to Figure 3

The red rectangles indicate amino acids from E1 that contribute major binding to MXRA8 while blue rectangles indicate amino acids from E1' that contribute minor binding to MXRA8. The red triangles indicate amino acids from E2 that contributed major binding to MXRA8 while blue triangles indicate amino acids from E2′ that contribute minor binding to MXRA8. GenBank Accession codes: CHIKV strain 05-115, CAJ90470; ONNV strain SG650, AF079456; RRV, strain T48, AAA47404; MAYV, AAL79764; BFV strain BH2193, AAB40702; SINV, NP_062890; VEEV strain TC-83, CAA27883.

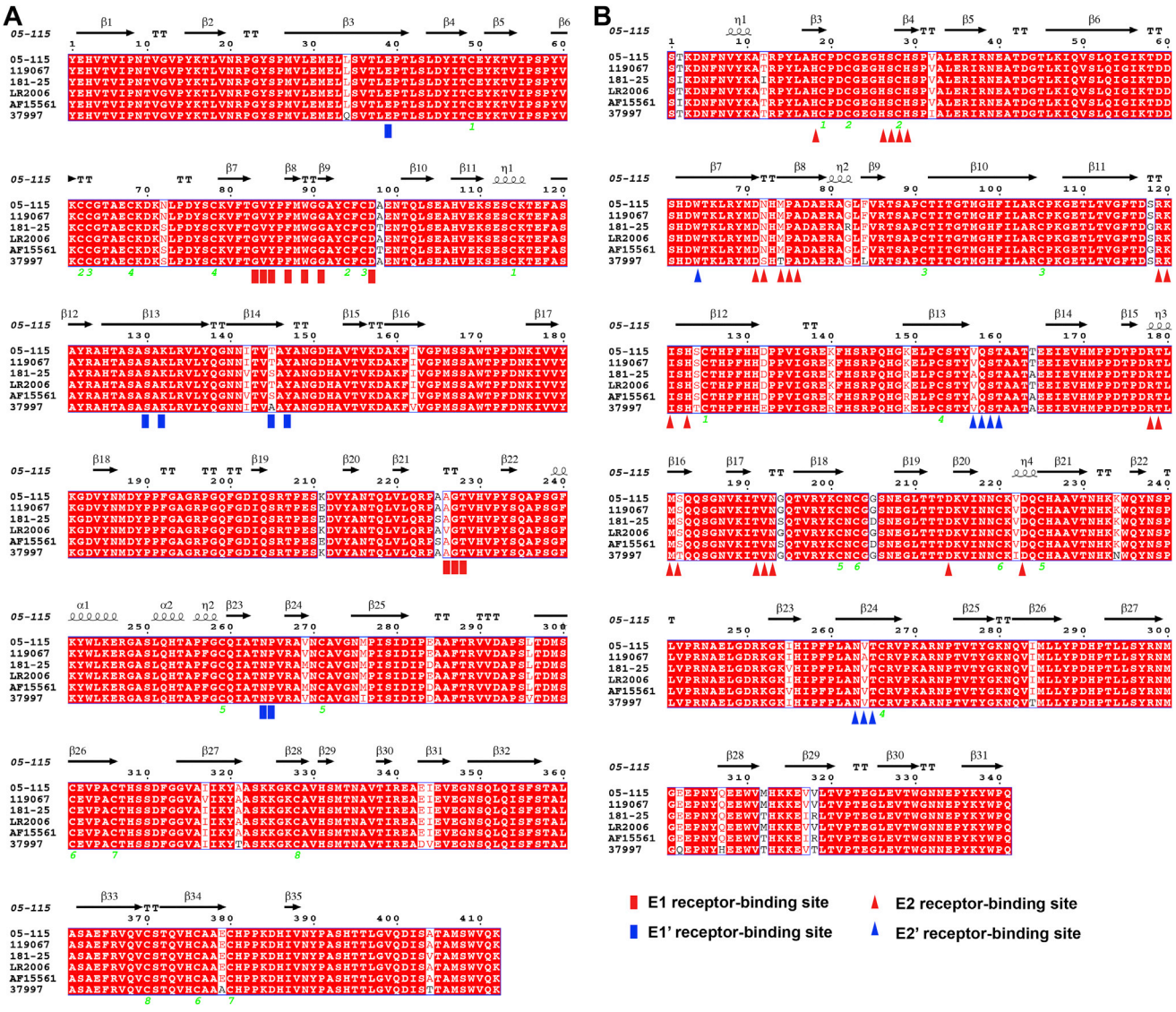

Figure S6. Sequence Alignment of E1 and E2 Proteins from Representative CHIKV Strains, Related to Figure 3

The red rectangles indicate amino acids from E1 that contribute major binding to MXRA8 while blue rectangles indicate amino acids from E1' that contribute minor binding to MXRA8. The red triangles indicate amino acids from E2 that contributed major binding to MXRA8 while blue triangles indicate amino acids from E2′ that contribute minor binding to MXRA8. GenBank Accession codes: CHIKV strain 05-115, CAJ90470; strain 119067, APA34057; strain 181-25, AAA53256; LR2006, DQ443544; strain AF15561, ABO38821; strain 37997, AAU43881.

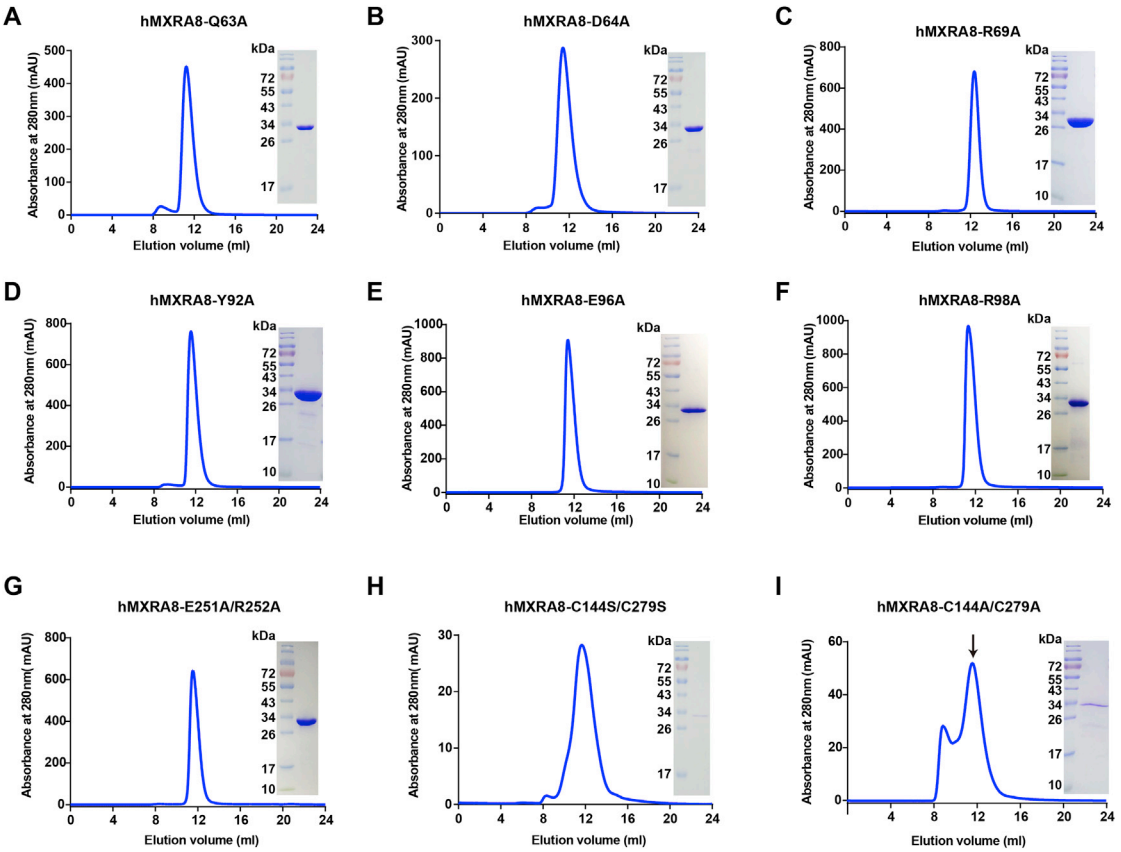

Figure S7. Biophysical Characterization of the hMXRA8 Mutant Proteins, Related to Figure 5

Analytical gel filtration of different hMXRA8 mutant proteins with Superdex® 75 10/300 GL. The 280-nm absorbance curve and the SDS-PAGE migration profile of the pooled sample are shown.